2018

Implementing simultaneous calcium imaging and optogenetics in freely moving rodents to investigate the role of local inhibition in place field stability

Helena Yan
hyan@wellesley.edu

Implementing simultaneous calcium imaging and optogenetics in freely moving rodents to investigate the role of local inhibition in place field stability

Helena Z. H. Yan

Off-campus Advisor: Matthew A. Wilson, MIT Department of Brain and Cognitive Sciences
Direct Supervisor: Jonathan P. Newman, MIT Department of Brain and Cognitive Sciences
On-campus Advisor: Sara Wasserman, Wellesley College Neuroscience Department
Additional Advisor: Michael C. Wiest, Wellesley College Neuroscience Department
Neuroscience Department
Wellesley College

May 25, 2018
This material is submitted as partial fulfillment of a B.A. degree with honours in Neuroscience

Acknowledgements

When I first entered Wellesley College, I had never heard of undergraduate students performing research, let alone writing theses. Almost four years later, I am surprised that I have been able to write my own senior thesis in neuroscience and know that it wouldn't have been possible without the encouragement given by my mentors, friends, and family. One page cannot show my gratitude for all of the support I've received, but I will try anyways:

To Jon Newman, for being the most supportive and encouraging mentor I could have had. From the moment I stepped into lab, you took me under your tie-dyed wing and taught me as much as I could learn. These past three years have passed by in a blur and you continue to inspire me with your dedication to detail and rigorous thought. I am so glad that I had the chance to do science with you, while learning new vocabulary such as "chooch" and "shmoo". Your support for me extended far beyond the lab and I don't know how I could have reached the end of these years without your guidance.

To Matthew Wilson, for welcoming me to his lab and traveling all the way to Wellesley each time I had a committee meeting. I used to wonder if you knew the name of that random Wellesley UROP who took over a desk in the office space without asking and am now sure that you do.

To James Demelo, for providing a never-ending supply of candy when I'm in lab and for giving me the final push in writing. Thank you for checking in every time I had a big surgery day, for comforting me when I was really stressed out during the summer, and for all the support in-between.

To Mike Wiest, for introducing me to the world of neuroscience research and for being on my thesis committee.

To Sara Wasserman, for always reassuring me when I was panicking, checking in on me every time we met, and being on my thesis committee.

To my friends, for all the memories in the science center and beyond that kept me sane during the thesis-writing process. Thank you for putting up with me being off-campus all the time, for letting me stay in your rooms overnight when I lived off campus and had an 8:30am class, and for the all-day thesis-writing session.

To my lab-mates, for being so accommodating when I used their behaviour rooms for experiments and for making the Wilson lab such a familiar group to work with.

To my research animals. Despite all the things I've put you through, you pooped and peed on me minimally. I am so sorry for any anxiety and pain that I have caused you and can only hope that the analgesics I gave you each time you had a surgery dulled the pain and made you feel warm and fuzzy.

And finally, to my family. Although it's hard to communicate my research through a language barrier, you have always supported me and encouraged me to pursue it, even when it meant less time spent with you at home.

Table of Contents

List of Figures

List of Equations

List of Tables

Abstract

Place cells are pyramidal neurons in CA1, 2, and 3 of the hippocampus that fire preferentially when an animal is located in a certain position in an environment. The location to which a place cell maximally responds (its place field) is randomly assigned within an environment. Place fields can be re-assigned depending on changes to local sensory cues within an environment, a phenomenon called "remapping". Research has established that place field formation is affected by input from the local network in the hippocampus. Interneurons in CA1 are known to provide inhibitory input into place cells, but no causal link between local inhibition and place map remapping has been demonstrated. Here, we sought to understand if directly driving local inhibitory networks in CA1 could induce place field remapping. To do this, we used optogenetic stimulation to excite interneurons while concurrently monitoring neural activity using a red-shifted calcium indicator (jRCaMP1b) in freely moving mice. Microendoscopic calcium imaging was performed over multiple days as the mouse explored an open field. After the animal had explored the field for several days, interneurons in CA1 were optogenetically activated at certain positions in the environment. Unfortunately, the low signal to noise level of the red-shifted calcium indicator prevented analysis of this dataset. In lieu of this, we analyzed data from a green fluorescent calcium indicator (GCaMP6f) that we used to initially test out our experimental technique. The results of this analysis revealed aberrant neural activity during calcium imaging sessions, suggesting that the calcium imaging technique may have unexpected, pathological effects on neural activity in the hippocampus. The work described here sets the groundwork for further concurrent use of optogenetics with calcium imaging in investigations into the cellular mechanisms behind place field formation.

Introduction

When Henry Molaison was a child, he experienced epilepsy which could not be controlled by any medications. The seizure episodes, which increased in severity as he grew older, originated from his medial temporal lobes (MTL). When he was 27 years old, Molaison underwent surgery to have his MTL removed bilaterally, in the hopes that it would cure his seizures. The procedure successfully removed the hippocampus, medial entorhinal cortex, and part of the amygdala, and Molaison's seizures stopped. However, because of the brain tissue removed, Molaison experienced deficits in explicit memory—he could not remember certain facts about his own life (like the death of a favourite uncle three years ago) and could not form any new memories.

Despite Molaison's extensive memory loss, he could still navigate novel environments after enough practice. Five years after his surgery, Molaison moved with his family to a new house. Although he had not been exposed to the layout of the house before his procedure, Molaison was eventually able to create detailed floor plans of his new home (Corkin, 2002), suggesting his spatial memory abilities were not lost. This ability was unexpected, as other patients who had bilateral damage to their hippocampus and medial temporal lobe were not able to recall the neighborhoods they had moved to after developing amnesia (Teng and Squire, 1999; Rosenbaum et al., 2000). However, the state of Molaison's spatial memory is controversial, as formal testing revealed chance-level performance of spatial location recall (Smith, 1988). After Molaison's death, researchers examined his brain to confirm the brain regions removed and discovered that portions of his hippocampus were not removed as initially expected, which may explain how he retained portions of his spatial memory (Annese et al., 2014). More importantly, the case study of H.M. demonstrates the importance of the hippocampus in forming new spatial memory.

The role of the hippocampus in spatial memory formation

Lesion studies done in rats support the hypothesis that the hippocampus is critically involved in spatial memory formation. In comparison to rats who had cortical lesions or control

rats, those who had their hippocampi aspirated did not perform as well on the Morris water maze task, as they were unable to learn the location of a hidden platform in a water maze after repeated trials (Morris et al., 1982). Further animal studies distinguishing dorsal and ventral hippocampal lesions demonstrated that the main region responsible for normal performance on the Morris water maze, and therefore for spatial memory formation, was the dorsal hippocampus (Bannerman et al., 2002).

A region called the Cornu Ammonis 1 (CA1) takes up most of the dorsal hippocampus and contains cells that are thought to be critical for the acquisition of spatial memory, called "place cells"(O'Keefe and Dostrovsky, 1971; Wilson and McNaughton, 1993). First discovered through cellular recordings in rats, place cells become active when the organism is in a specific place within an enclosed environment (O'Keefe and Dostrovsky, 1971). The places in the environment where a specific place cell is active is referred to as a "place field". The activity of thousands of these cells across a spatial environment collectively form a "place map". This map is likely used by the organism to infer its position relative to salient sensory landmarks within an environment, for instance visual, auditory, and olfactory cues (Maaswinkel and Whishaw, 1999). The activity of the cells comprising this map are thought to be critical for both real-time position estimation during foraging as well as acquisition (Hasselmo et al., 2002) of spatial memory following navigation (Wilson and McNaughton, 1994).

Place fields can change

Unlike the organization of the visual system, where there is a correspondence between neurons in the visual cortex and the visual field, place cells do not appear to be organized by their place fields. Two adjacent cells can have place preferences for either ends of the environment in one instance and have place fields right next to each other in another environment. Place fields are formed based on a complex combination of factors in the environment. Most studies into the factors influencing place map stability involve monitoring place cell activity while an animal is exploring an

enclosed space, marked with landmarks (Muller and Kubie, 1987; O'Keefe and Burgess, 1996; Lever et al., 2002).

These studies into place map stability aim to see whether place fields change their spatial preferences within the same environment—commonly called "remapping". Experiments have shown that place fields often remap when spatial relationships between salient cues are changed. For example, in a completely empty circular environment encircled by a grey wall, changing the placement of the single white cue card present on the wall rotated place fields, despite the maze walls not shifting position with respect to the rest of the room (Muller and Kubie, 1987). The same study also distorted the environment by scaling up the diameter of the circular environment and the height of the walls and found that a third of the place fields stretched along with the environment, so that their angular and radial positions remained the same. Whether the place fields remap also depended on whether the animal witnessed the environment changing or not. A separate study in rats found that place fields only rotated with a moving cue when the animal did not know that the cue was moved (Jeffery and O'Keefe, 1999).

When an environment's cues remain unchanged, there is still variation in place fields from day-to-day. However, place maps are preserved in spite of this daily variation, so the place map observed on any given day can still be used to interpret place cell activity and infer the animal's location one month after the reference day (Ziv et al., 2013).

Place fields can contain multiple points in the same environment

While it is easiest to think of each place cell being active in just one spot within an environment, place cells can represent multiple positions within an environment (Rich et al., 2014). When rats were run on long linear tracks, researchers found that the same place cell was active at multiple points along the track and that these points were randomly spaced (Rich et al., 2014). Therefore, place fields do not form in a predictable pattern.

One important note is that place field remapping is not the same as place fields changing between environments. In studies that have exposed animals to separate configurations of visual cues within a single environment, rapidly switching the cues from one configuration to the other resulted in place fields flickering between the two representations, before settling on the field for the current configuration (Jezek et al., 2011).

The winner-takes-all model of spatial memory formation

While most of the past research into spatial memory formation has focused on how an animal's experience influences the representation of an environment (Muller and Kubie, 1987; Maaswinkel and Whishaw, 1999; Zhang and Manahan-Vaughan, 2015), attention is now being turned to investigating how the representations are generated on a cellular level. In a study involving a linear track, silent place cells were depolarized via a constant current injection while their activity pattern was observed (Lee et al., 2012). These previously silent cells became active when the animal encountered specific positions on the linear maze, suggesting that they may have formed a place field (figure 1).

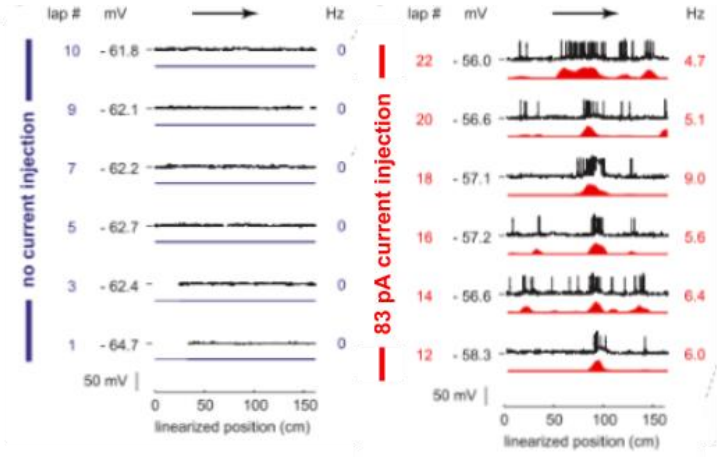

Figure 1. Previously silent place cells became active in a spatially-linked manner following constant current depolarization of cell somas. Rats were implanted with a patch clamp in the dorsal CA1 region and placed on a circular "o"-shaped track to freely explore. After at least two laps, if the cell targeted by the patch clamp was not active, a constant current was injected with increasing voltage to depolarize the cell. During current injections, the cell's activity was recorded using the same patch clamp. Figure adapted from Lee et al. (2012).

One explanation for this observation is that the constant current injection resulted in depolarization that freed the place cells from local inhibition, so that they became more easily excitable. This supports the winner-takes-all model of neural computation, which posits that the presence of excited neurons in a large network can discourage more neurons from becoming

excited. Place cells that are activated by sensory input provide excitatory input into interneurons and thus increase the inhibition of the overall population. Current injection removes the source of inhibition on the place cells and thus disrupts the winner-take-all process, therefore freeing more cells to develop a spatial spiking preference.

The winner-takes-all theory is supported by observations of place cell activity during initial place field formation and studies perturbing cells in the network. Place map formation involves an initial period where place cells are more active than usual (Epsztein et al., 2011) and interneuron activity is lower than normal (Wilson and McNaughton, 1993). This period of low inhibition makes it harder for any neuron to influence the activity of the entire population and explains how the high place cell activity can arise from the cellular network. Similarly, inhibiting place cells lead to new place fields replacing the old ones, while inhibiting interneurons increased the rate of place cell firing without place field remapping (Schoenenberger et al., 2016). Therefore, place cells seem to only develop new place maps when their activity is inhibited.

The proposed experiment

While it is clear that place cell activity and place map formation are affected by input from interneurons (Schoenenberger et al., 2016), the causal link between the two is has not been demonstrated. Until now, studies have only manipulated the activity of place cells directly or decreased interneuronal input into place cells. Therefore, further work is still needed to investigate whether local inhibition is sufficient to induce remapping. My proposed study aims to address this need through optogenetic excitation of interneurons with concurrent calcium imaging of place cell activity.

Research methods used to record cellular activity

Traditionally, studies of rodent place cell activity in relation to spatial memory relied on electrophysiological recordings to measure place cell activity (O'Keefe and Dostrovsky, 1971). This remains the main technique used in the field. While electrophysiological technologies have

improved dramatically in the last few decades (Cogan, 2008; Kim et al., 2013; Patil and Thakor, 2016), there are weaknesses in the technique that are especially relevant to the recording of place cell activity over long time periods. Namely, the electrodes used in electrophysiological recordings can shift position over time, referred to as "electrode drift" (Pachitariu et al., 2016), which may result in different cells being recorded day-to-day. Since place fields are a property of individual cells, incorrectly assigning activity from different cells to one cell will lead to the incorrect conclusion that place fields have changed during the recording time. Therefore, any research technique used to record place cell activity must accurately identify cells and keep track of those cells over the experimental period.

Recording long-term cellular activity using calcium imaging

Calcium imaging is a relatively new technique that addresses the major weakness of electrophysiological recordings. Using indicator molecules that change their fluorescence when bound to calcium, cellular activity can be monitored using a camera sensor (Ghosh et al., 2011). Using this technique, long-term observation of the same cells is easier since the frame of view on the camera sensor theoretically stays the same throughout the animal's lifetime and processing can be performed to account for small movement artifacts in collected video (Pnevmatikakis and Giovannucci, 2017). Additional benefits to calcium imaging include a larger cell yield in comparison to electrophysiological recordings and the ability to record from specific neural populations via cell-type-specific expression of calcium indicators.

The most widely used fluorescent indicator is GCaMP, which contains a green-fluorescent protein (GFP) fused with calmodulin and a peptide from smooth-muscle myosin light-chain kinase (RS20) (Nakai et al., 2001). Calcium ions induce calmodulin to bind to RS20, which increases the fluorescence of the GFP molecule it is bound to (Figure 2) (Schoenenberger et al., 2016). Since intracellular calcium levels increase whenever an action potential is fired, the natural influx of calcium into the cell increases the fluorescence of GCaMP and thus can be used as a measure of

neuronal activity. GFP fluorescence can be detected by exciting GFP molecules with blue light and measuring the emitted green light with a camera sensor (Chen et al., 2013).

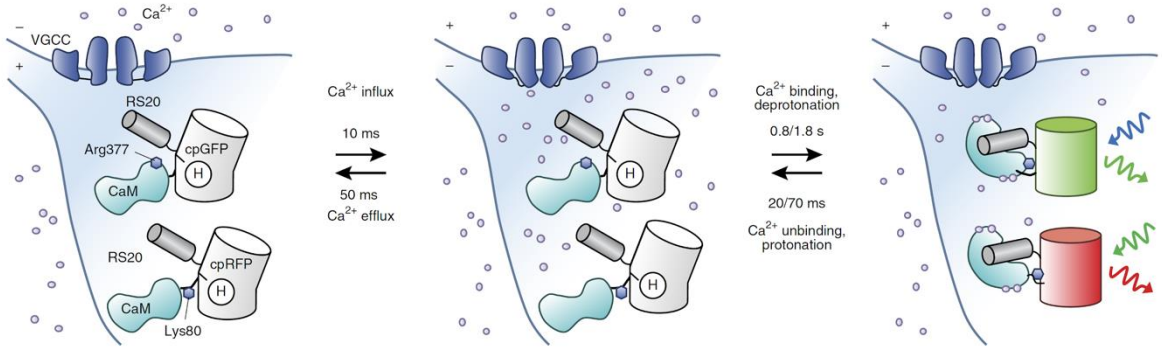

Figure 2. Mechanism of action for GCaMP proteins. Once there is a calcium influx, calcium ions bind to the calmodulin domain of the GCaMP protein. This induces the RS20 domain to bind to calmodulin, which in turn changes the conformation of the GFP protein linking both domains, thus increasing GFP fluorescence. Taken from (Lin and Schnitzer, 2016).

While calcium imaging enables more accurate cell identification across days, its main drawbacks are that its slow kinetics make it difficult to extract spike activity from the raw video data. Further, when used with widefield imaging technique, the data contain out-of-focus background fluorescence.

Manipulating cellular activity using optogenetics

Investigating if interneuron inhibition is sufficient to induce new place map formation required a way to perturb the interneuron population activity. Ideally, this method should allow stimulation of a large group of interneurons at a biologically relevant timescale and not interfere with calcium imaging. Optogenetics uses a light-sensitive ion channel to influence cellular activity. Channelrhodopsin 2 (ChR2) is the main excitatory channel used in optogenetics and is composed of a light-sensitive opsin molecule attached to a non-specific cation channel (Boyden et al., 2005). The opsin molecule is most sensitive to blue light (~480nm) and changes conformation to open the channel when stimulated (Boyden et al., 2005; Zhang et al., 2006). Since ChR2 has around one millisecond dynamics, it is commonly used to stimulate neurons.

Conveniently, the light path used for calcium imaging can be modified to support optogenetic stimulation hardware. However, one major problem in combining calcium imaging with optogenetic stimulation is the risk of overlapping excitation wavelengths. Since GCaMP and ChR2 are both excited by blue light, imaging calcium activity in a ChR2-expressing animal would automatically lead to optogenetic stimulation. To avoid overlapping excitation spectra, we used a red-shifted calcium indicator called jRCaMP1b, which emits red light when stimulated by green light (Dana et al., 2016) and the standard ChR2, which is excited by blue light.

Red-shifted Calcium Indicators

Similar to GCaMP, red-shifted calcium indicators like RCaMP contain a red fluorescent protein, calmodulin, and RS20 (Dana et al., 2016). For my experiments, I will be using jRCaMP1b, which has one of the fastest decay kinetics and calcium affinities of all RCaMP molecules (Dana et al., 2016). jRCaMP1b still is slower than GCaMP6f in its decay, does not have as high a maximum emission peak as GCaMP6f (Figure 3) and has a shallower increase in fluorescence as stimulation frequency increases (Figure 4). Whereas the slower decay dynamics of the RCaMP may make the data analysis more difficult, the ability to use RCaMP and ChR2 simultaneously provides a novel opportunity to simultaneously perturb neural activity and observe its effects.

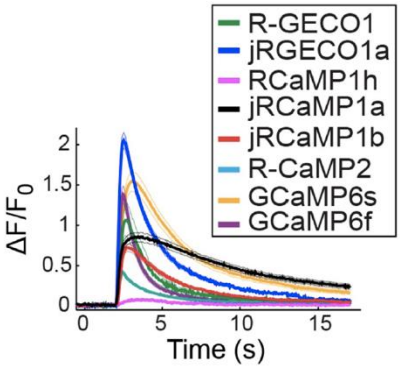

Figure 3. jRCaMP1b has a smaller peak signal level than GCaMP6f. Plasmids containing the genetic material of various calcium indicators were injected separately in zebrafish larvae. The larvae were paralyzed, embedded in agarose, and stimulated with five pulses at 20Hz. Response fluorescence amplitudes were observed in the zebrafish trigeminal neurons. Adapted from Dana et al (2016).

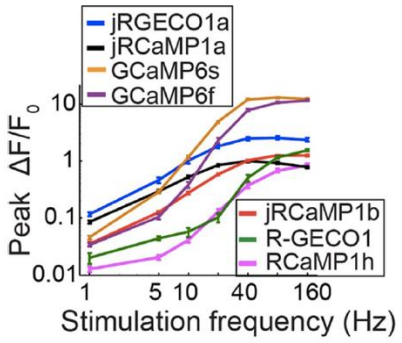

Figure 4. jRCaMP1b has a shallower frequency-tuned response in comparison to GCaMP6f. Various calcium indicators were expressed separately in the neuro-muscular junction of Drosophila larvae using transgenic flies. The segmented motor nerve of the larvae was stimulated while the fluorescent activity was measured at the presynaptic bouton. Adapted from Dana et al (2016).

Calcium Signal Analysis

To infer neural activity from widefield fluorescence levels measured with a camera sensor, one needs to identify the outline of each active cell within the video frame (referred to as the "spatial footprint"), distinguish background fluorescence from the fluorescence associated with neural activity, and take into account the kinetics of the fluorescent molecule when back-calculating the spiking activity. Pnevmatikakis et al. (2016) have created a calcium imaging analysis suite (CaImAn) that approaches these three challenges from a mathematical modelling perspective.

They model the fluorescent activity observed in the video frame at any given time, y(t), as a weighted sum of the calcium concentration due to spiking activity, c(t), the baseline calcium concentration, b, and the noise, $\epsilon(t)$ (see equation 1). In the equation below, α is a nonnegative scalar and the noise is assumed to be constant and have a gaussian distribution.

$$y(t) = \alpha(c(t) + b) + \epsilon(t),\ \epsilon(t) \sim N(0, \sigma^2)$$

Equation 1. Observed fluorescence modeled in relation to calcium concentration. y(t) is the fluorescence activity observed, is a nonnegative scalar multiple, c(t) is the calcium concentration due to spiking activity, b is the baseline calcium concentration within the cell, and $\epsilon(t)$ is the noise in the observed fluorescence. From Pnevmatikakis et al. (2016).

A few assumptions are made so that the above equation can be solved through numerical optimization. First, the spiking activity is assumed to be greater than zero (that is, the raw video is assumed to contain spiking cells). Second, the spike-related calcium activity is assumed to be due to the simplest (sparsest) combination of spiking activity. Third, while the spatial footprints of

different cells can overlap, individual spatial footprints are assumed to be as sparse and compact as possible while still accurately capturing the data. Lastly, due to our inability to determine the value of α, the scalar multiple of spike-related calcium activity, only a relative firing rate can be extracted from the fluorescence.

Cell Tracking Across Days

Since our experiments require comparing place fields and place cell activity between days, we needed a way to keep track of the same cell between different videos. The main challenge in analyzing multi-day endoscopic calcium imaging data is accounting for the day-to-day shifts in the visual field. The method used to register cells across days in this project is called Cell Reg (Sheintuch et al., 2017). Using multiple days' worth of spatial footprints produced by the CaImAn, Cell Reg calculates the distance between centers of mass of the spatial footprints and the Pearson correlation between the spatial footprints of cells in a local neighborhood ("spatial correlation").

Upon plotting the distribution of centroid distances and spatial correlations, a bimodal distribution is observed (Figure 5), which visually isolated two subpopulations of spatial footprints. Sheintuch et al. (2017) modelled the observed distribution of centroid distance and spatial correlation as the sum of two subpopulations. The group that has low spatial correlation and large centroid distance are most likely different cells while the group with high spatial correlation and small centroid distance are most likely the same cell. Using that model, one can calculate P_{same}— the probability that 2 cells from two different recording sessions are the same cell—from the spatial correlation and centroid distance values. By setting a minimum threshold for P_{same}, one can sort the spatial footprints of each day into either the same cells or different cells.

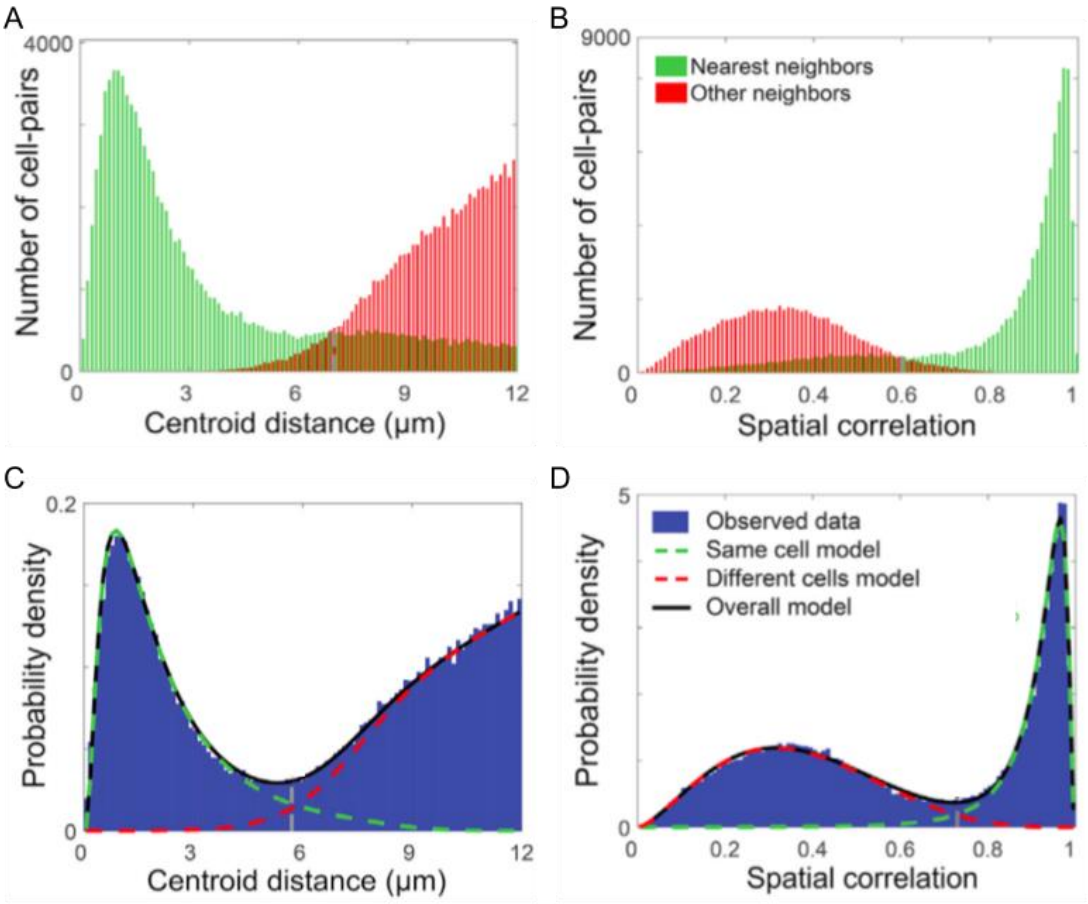

Figure 5. Neighboring cell pairs can be modeled as a bimodal distribution composed of subpopulations of same-cell pairs and different-cell pairs. Spatial footprints of cells were extracted from multiple days' worth of calcium activity video. Each spatial footprint was projected into all the days' video frame to identify cells in each other's vicinity. Distribution of centroid distances (A) and spatial correlations (B) were compared between sessions and modeled as the sum of two subpopulations: same-cell pairs (green dashed line) and different-cell pairs (red dashed line) in graphs C and D, respectively. Figure adapted from Sheintuch et al., 2017.

Statement of objectives

This study aims to investigate the hypothesis that interneurons can induce place map formation by providing inhibitory input to place cells. To test this hypothesis, we will be using a red-shifted calcium indicator, jRCaMP1b, to record neural activity of individual neurons in animals roaming around an open field maze. Concurrently, we will optogenetically excite the interneurons to examine their effect on place field stability.

Materials and Methods

Animals

All experimental protocols were approved by the Committee on Animal Care at Massachusetts Institute of Technology (MIT). Animals were maintained in MIT's Animal Care Facility on a 12 hr/12 hr light/dark cycle. The mice were housed with littermates upon weaning and transferred to individual cages after the first surgical procedure. Each cage contained cotton pads for nesting material, as well as food and water ad libitum.

Three strains of mice (*Mus musculus*) with C57BL/6 genetic background were used to breed the experimental mice: Ai32, VGAT-Cre, and PV-Cre. Ai32 mice (Jackson Laboratories, stock #024109) express a ChR2/EYFP fusion protein following exposure to Cre recombinase. VGAT-Cre mice (Jackson Laboratories, stock #028862) express Cre recombinase in inhibitory GABAergic neuron cell bodies. PV-Cre (Jackson Laboratories, stock # 017320) express Cre-recombinase in parvalbumin-expressing neurons, which includes a subset of interneurons. Experimental animals were male or female mice that were either VGAT-CrexAi32 or PV-CrexAi32.

Animal husbandry

Male homozygous Ai32 mice were housed with either two homozygous VGAT-Cre or two homozygous PV-Cre mice, to produce heterozygous VGAT-CrexAi32 or PV-CrexAi32 pups (Fig. 6). Pups were weaned and genotyped at three weeks old.

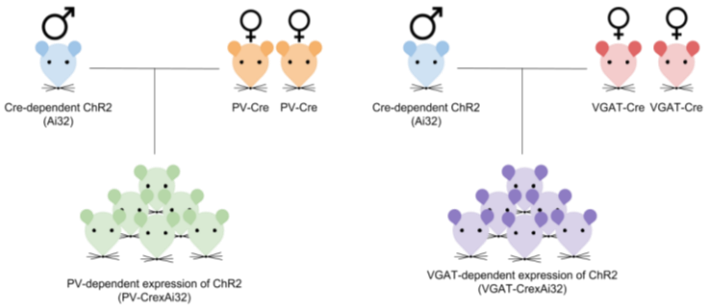

Figure 6. Breeding scheme for ChR2-expressing animals. Male mice that are homozygous for a Cre-dependent ChR2 gene are crossed with homozygous females expressing Cre in either PV or VGAT cells. The offspring are heterozygous, having either PV-dependent or VGAT-dependent expression of ChR2.

Opto-G-scope: a fluorescent microendoscope with an integrated optogenetic stimulator

The filter tube of the opensource UCLA miniscope (Cai et al., 2016) was elongated to include space for an additional excitation LED and dichroic mirror for optogenetic stimulation. The modified miniscope, nicknamed the "opto-G-scope", contained two excitation LEDs—one green for calcium imaging, and one blue for optogenetic stimulation (Fig. 7). The filters used in the opto-G-scope include an excitation filter for the green LED (ET560/40x), an emission filter (Chroma ET630/75m), and two dichroic filters to filter and direct the light (Chroma T495lpxr and T585lpxr). An achromatic lens (Edmund Optics, catalog # 45-207) was used to focus the incoming parallel light rays onto the sensor (figure 8). These light rays came from a gradient-index lens ("GRIN lens"), whose index of refraction is a function of radial position in the cylindrical lens. Magnets were glued to the bottom of the scope body to allow for easy attachment to the traditional aluminum mounting plate ("baseplate") for in-vivo imaging.

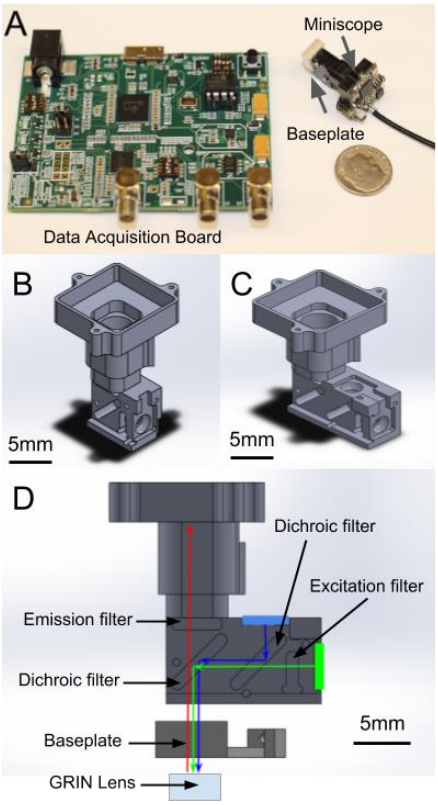

Figure 7. Overview of the miniscope and opto-G-scope. (A) A baseplate is glued to the animal's skull so that the miniscope can be attached. The miniscope interfaces with the computer via the data acquisition board. **(B)** Design of the plastic case of the miniscope, which contains three slots for optical lenses, a place for an LED light at the right end of the bottom piece, a sliding body to allow for focusing, and a mount for a camera sensor at the top. **(C)** Design of the plastic case of the opto-G-scope, which contains an additional slot for an optical lens and an additional place for the optogenetics stimulating LED. **(D)** A diagram showing the light paths within the opto-G-scope. The green rectangle is the green LED for stimulating RCaMP, the blue rectangle is the blue LED for stimulating ChR2. Only red wavelengths pass through the emission filter to reach the camera sensor at the top.

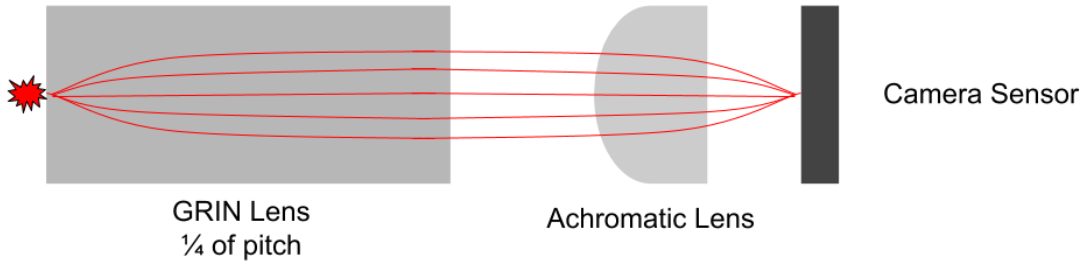

Figure 8. Schematic of light rays passing through a GRIN lens. The index of refraction within a GRIN lens is a function of radial position in the cylinder. Since light bends sinusoidally with a well-defined period in a GRIN lens, cutting the lens to a quarter of its pitch will turn light rays emitted at one point on one end of the lens (red star) into parallel beams exiting the other end of the lens.

Surgical procedures for calcium imaging

The following procedures were adapted from techniques developed by the Golshani and Silva labs (Cai et al., 2016). Animals were given 1.0mg/kg of slow-release buprenorphine at the start of any invasive procedure.

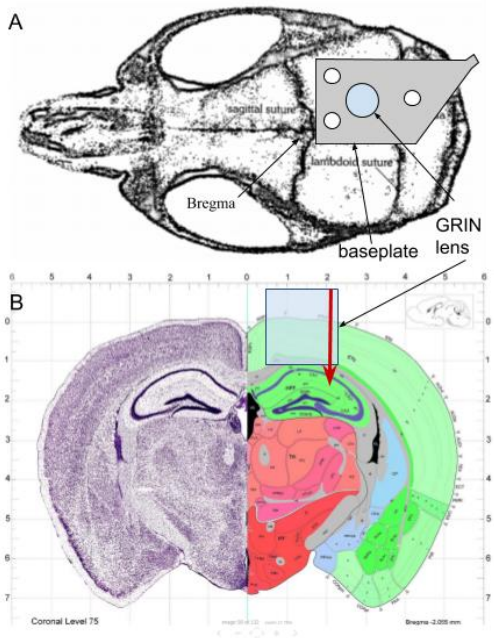

Figure 9. Overview of all surgical procedures for calcium imaging. Virus containing the genetic material for calcium indicators is injected lateral to the imaging site to minimize the amount of damaged tissue being imaged. Following aspiration of portions of the cortex, a gradient index (GRIN) lens is implanted above CA1 of the hippocampus. Lastly, a baseplate is glued to the skull to allow for easy attachment of the miniscope for imaging sessions. **(A)** A dorsal view of the mouse skull with all surgical procedures visualized. **(B)** A coronal view of the mouse brain (2.055mm posterior of bregma) with all surgical procedures visualized. Image of brain slice from Allen Online Brain Atlas.

<u>Viral injections</u>

To express calcium indicators in the target cell population, viral injections were used to deliver the calcium indicator gene to experimental animals. 0.5ul of GCaMP6f (Penn Vector Core,

AAV1.Syn.GCaMP6f.WPRE.SV40) at 1.00x10 ^13 genome copies (GC)/ml or 0.5ul of jRCaMP1b (Penn Vector Core, AAV1.Syn.NES-jRCaMP1b.WPRE.SV40) at 6.69x10^13 GC/ml were injected into the right dorsal hippocampus (-2.1mm posterior, 2.1mm right of, and -1.7mm dorsal to bregma) when animals were at least 2 months old (figure 9).

Lens implants

Two weeks after the viral injection surgery, mice were implanted with a gradient-optics lens ("GRIN lens"; Edmund Optics, catalog #64-519). A craniotomy was made at -2.1mm posterior and 1.5mm right of bregma and brain tissue is aspirated to a depth of -1.35mm (figure 9B). The GRIN lens was lowered into the bottom of the craniotomy and secured to the skull via a head cap made with cyanoacrylate glue (Starbond EM-02), cyanoacrylate gel (Loctite 454 Prism Gel Adhesive) and dental acrylic (Contemporary Ortho-Jet Powder, black).

Baseplating

Three to four weeks following the implant surgery, cells are imaged through the GRIN lens using an opto-G-scope. The angle, position, and focus length of the scope is manually adjusted over the GRIN lens until cells can be clearly seen. Additionally, we try to include blood vessels in the field of view to act as static landmarks that are useful during motion correction. Upon finding satisfactory position, the aluminum baseplate is glued to the head cap to preserve the field of view and the focus adjustment set screw tightened in place (figure 9A). Following baseplating, the opto-G-scope can be attached and detached from the animal's head using a set of inset magnets during behavioural experiments to achieve the same field of view day-to-day.

Behavioural experiment

Each animal was exposed to a control environment, where there were no perturbations to the environment, and an experimental environment, where they experienced a perturbation. The environments were made of white corrugated plastic, with 30cm tall walls forming a four-sided polygon. Each wall had a differently-shaped cue on it, made with black contact paper.

Experimental periods were divided into three stages: pre-perturbation, perturbation, and post-perturbation. In the pre-perturbation stage, calcium activity was recorded for 15 minutes while the animal was exploring the environment. In the perturbation stage, calcium activity was recorded while the animal experienced an altered environment. In the post-perturbation stage, animals were placed into their respective environments and calcium activity was recorded for 15 consecutive minutes.

Recording Rig Design

A mobile recording rig, comprised of a computer, the recording frame, and detachable mazes (see next section for details), was used for data collection (figure 10). The recording frame was made of extruded aluminum "t-slot" bars (111cm tall) and held the overhead behaviour camera, along with the data acquisition circuit that served as the interface between the miniscope and the computer, and a coaxial commutator to allow the miniscope tether to be untwisted during freely moving behavior. The base of the recording frame was attached to a plywood board (76cm x 75cm) that also served as the base for attaching the mazes.

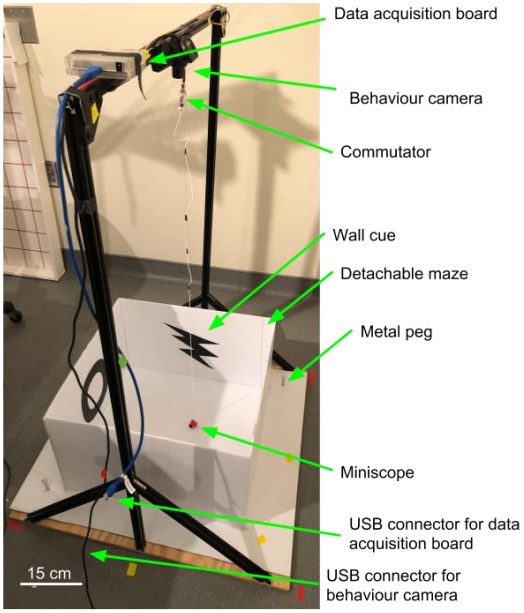

Figure 10. A labelled diagram of the recording rig. The metal frame (111cm tall) held the behaviour camera and data acquisition board. The miniscope was connected to the data acquisition board through a commutator and suspended from the metal frame. Two USB connectors interfaced with the data collection computer, one for the miniscope's data acquisition board and one for the behaviour camera. The mazes were detachable (76cm x 68cm) and secured to the wooden base of the recording rig with metal pegs inserted through holes in the plastic base of the mazes.

Maze Design

Mazes were made from white corrugated plastic. Each maze was a simple, convex quadrilateral, with approximately 2500 cm^2 area. Each of the four walls was decorated with a different visual cue made of black contact paper. The walls were held together using hot glue and attached to a floor of the same material. Holes were drilled into each of the four corners of the base board, so as to align with the holes in the wooden base, and metal pegs were used to secure each detachable plastic maze to the plywood base for each behavioural session. Each maze had distinct allocentric cues as well, as they were placed amongst 2-3 different rooms. One room was divided into 2-3 distinct recording regions using a black curtain and a table.

Data Collection

Data collection was performed using Bonsai, an open-source software created to process heterogenous streams of data (Lopes et al., 2015) using a plugin developed by Dr. Jonathan Newman (https://github.com/jonnew/Bonsai.Miniscope). Data was collected from two cameras: a behaviour camera mounted to the frame of the recording rig and the imaging sensor of the miniscope. For each frame of behavioural video collected, Bonsai extracted the location of the animal by tracking the location of the large red sticker on top of the miniscope and calculated its speed (figure 11). If the animal was designated for optogenetic stimulation, stimulation would be delivered when the animal was within a certain third of the maze and moving above a minimum speed. The trigger for the optogenetic stimulation was given by Bonsai, delivered to a Cyclops LED driver (Newman et al., 2015), which provided the current for the optogenetics LED.

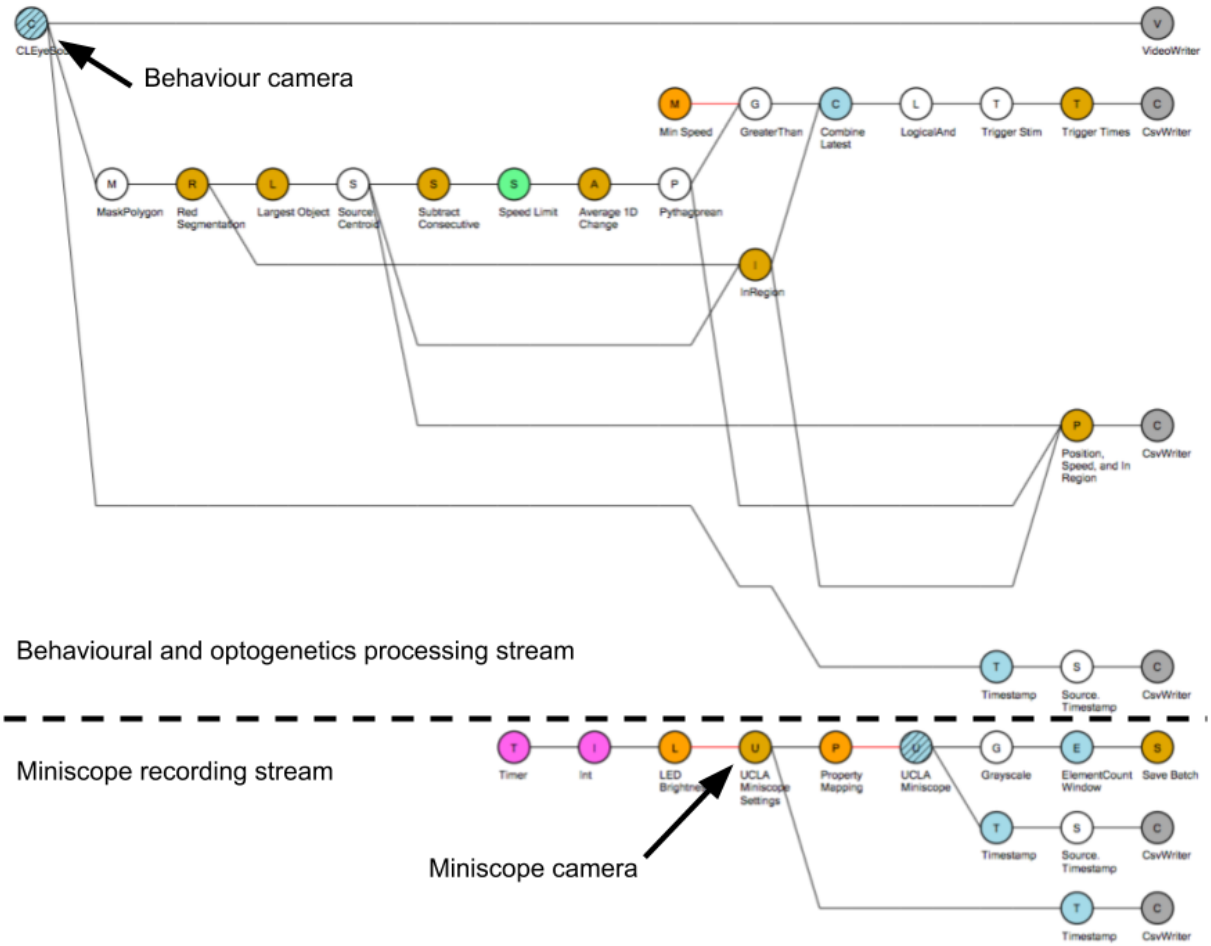

Figure 11. Recording workflow used in Bonsai. Bonsai acquired two video sources and saved seven different files: the raw behaviour video, the raw calcium activity video, time stamps for each frame of video collected, the speed for the animal calculated through Bonsai, and the miniscope settings used during each recording session.

Preliminary image analysis with ImageJ

To produce figures 12 and 13, videos of calcium activity from the first day of recording for each animal were examined using ImageJ, an opensource image processing program (Schindelin et al., 2012). Video files were loaded as a stack of tiff images and a projection of maximum intensity was created by selecting “Image>Stacks>Z-project>Max Intensity”. These maximum intensity projections were used to identify putative neurons. One such neuron identified was outlined using the ellipse tool and a plot of intensity over time was created by selecting “Image>Stacks>Plot Z-axis Profile”. A plot of intensity over time was also created for a section of the background of the same size as the neuron outlined.

Calcium Data Analysis

RCaMP activity recorded during behavioural sessions were processed using the CaImAn analysis suite (Pnevmatikakis et al., 2016). To identify the optimal parameters for analysis, a parameter sweep was done with the variables listed in table 1. The final parameter values used to analyze all data collected is also listed in table 1.

Table 1. Variables used in CaImAn that were optimized in the parameter sweep.

Variable	Values tested	Value used	Description
Gsig	2, 3, 5, 10	2	The diameter of a neuron in the calcium activity video. Width of Gaussian kernel used to spatially smooth data before determining areas of high local correlation, which are used as putative neurons to seed the algorithm.
Gsiz	4, 5, 6, 7, 8	5	The size of the background ring around each neuron identified. Used to model the local background fluorescence around the neuron.
Merge_thresh	0.6, 0.7, 0.8	0.75	The threshold value for spatiotemporal correlation that is used to determine whether two neighboring spatial footprints should be merged together to form a single neuron.
Neurons_per_patch	10, 50, 100, 200	200	Related to the maximum number of neurons that are allowed to be identified in each video. Whole video frames are divided into patches so that parallel processing can be used to speed up the processing time. Each patch can have a maximum of neurons_per_patch cells.
Nb_patch	8, 16, 32	16	The maximum number of background components used to model the static background of the video. Similar to how a Fourier series represents a function as the sum of multiple sine waves, the static background image of videos is represented as a weighted sum of gaussian sources of background fluorescence.

Alternate calcium data analysis from Ziv et al. (2013)

For the GCaMP6f fluorescence data collected, one day's activity analyzed by CaImAn was also processed using an alternate analysis outlined in Ziv et al. (2013). Rather than deconvolving the spiking times from the calcium signal, they defined calcium transients due to neural activity as peaks in fluorescence greater than two standard deviations from the baseline fluorescence. Following video denoising, these peaks in fluorescence were identified for each neuron's spatial

footprint (generated from the CaImAn analysis). Place fields were then created by correlating the times of calcium transients with the animal's location.

Confirmation of implant/imaging sites

At the conclusion of behavioural experiments, animals were transcardially perfused with 1x phosphate buffered solution (1xPBS) followed by a 4% formalin solution. Their brains were stored overnight in a 4% formalin solution and then sliced into 50um coronal sections. Slices were mounted with mounting medium containing DAPI (Vector Laboratories, catalog # H-1200). Slides were imaged using a Nikon TE2000 widefield microscope using brightfield, DAPI, TRITC, and FITC filters at 2x and 10x magnification to confirm implant and imaging sites and tissue health.

Ad hoc analysis of abnormal bursting activity

The start of abnormal bursting activity was identified in the collected GCaMP data by summing the amplitude of all traces produced by CaImAn, calculating the Z-score for each summed value, and identifying the times at which the Z-score of the summed amplitude exceeded 2. Correlations with animal behaviour were made by inspecting animal position 2 seconds before and after the onset of each identified burst.

Results

Implementing GCaMP calcium imaging

To verify the functionality of our behavioral setup and imaging system, we started by imaging GCaMP in wild-type animals. GCaMP is ~10x brighter than RCaMP and therefore allowed us to troubleshoot our experimental apparatus with more confidence than a weaker indicator. Wildtype mice were injected with virus containing genetic material for GCaMP6f (Chen et al., 2013), implanted with a GRIN lens, and affixed with a baseplate. Following recovery from baseplating, the animal was habituated to human handling and placed in an open field maze to freely explore. Calcium activity in CA1 was imaged using a conventional UCLA miniscope during this exploration (Cai et al., 2016). Videos were processed using ImageJ and active cells were identified within the video (figure 12).

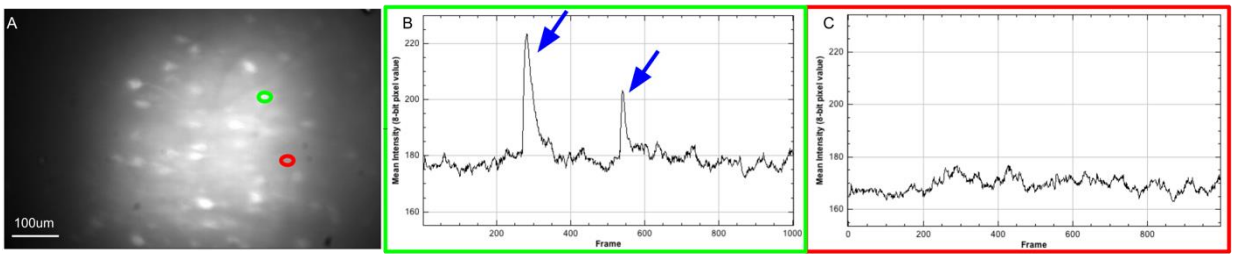

Figure 12. GCaMP Activity. A video of raw GCaMP activity was collected from a GCaMP-expressing mouse and processed using ImageJ. **(A)** A projection of maximum intensity of each pixel over all video frames yielded outlines of active cells. **(B)** A time series of intensity, measured in 8-bit pixel values, for a region of interest (circled in green in A) thought to be a neuron upon visual inspection of the video. Blue arrows indicate likely spikes in activity of the neuron **(C)** A time series of intensity, measured in 8-bit pixel values, for region of interest not thought to contain a neuron upon visual inspection of the video (circled in red in A). All videos had a 30Hz frame rate.

Implementing RCaMP calcium imaging

Following successful GCaMP calcium imaging in wildtype mice, ChR2-expressing mice were transfected with jRCaMP1b (Dana et al., 2016) and underwent the same surgical and imaging procedures. Although jRCaMP1b was expressed within cells of CA1 (figure 13), spikes in RCaMP fluorescence were much harder to distinguish from background fluorescence than in the GCaMP model.

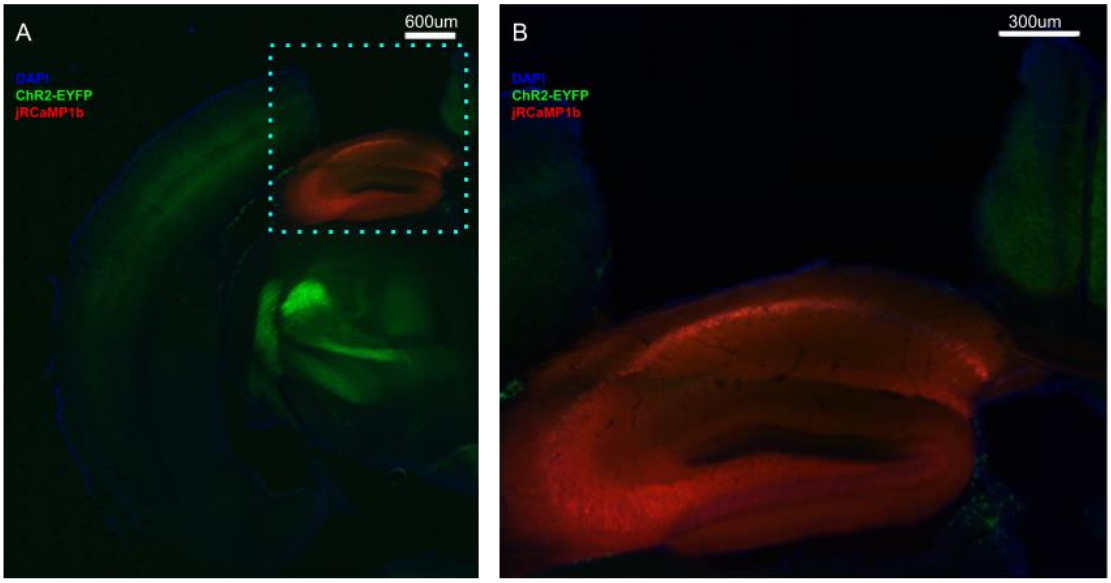

Figure 13. Histology of ChR2-expressing animal infected with jRCaMP1b. jRCaMP1b was injected into the hippocampus of a mouse expressing ChR2 in parvalbumin-expressing neurons. After behavioural experiments, the animal was euthanized, and the brain sectioned in 50um increments. The slices were mounted with a mounting medium containing DAPI and imaged at **(A)** 2x, scale bar is 600um and **(B)** 10x image of the region in (A) outlined in blue, scale bar is 300um. Blue is DAPI stain, green is ChR2-EYFP fluorescence, and red is jRCaMP1b fluorescence. Imaged slice is 2.1mm posterior to bregma, right under the center of the craniotomy and the GRIN lens implant site.

The changes in fluorescence levels were visibly slower and active cells were hard to identify by eye (figure 14A). Video analysis using ImageJ supported this observation, as the fluorescent intensity of neurons had a low signal to noise ratio and it was hard to distinguish neurons from background when looking at plots of the intensity changes over time (figure 14B-C). Poor signal quality persisted even when we increased the brightness of the excitation LED for jRCaMP1b. As the analysis depended on the quality of the video data, we chose to process the videos of GCaMP6f activity first before those of jRCaMP1b. Due to time constraints of this thesis project, only analyses from the GCaMP data were performed.

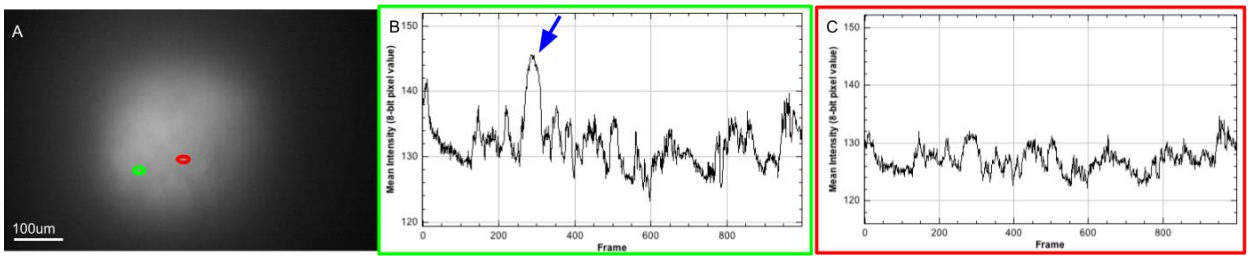

Figure 14. RCaMP Activity. A video of raw RCaMP activity was collected from an RCaMP-expressing mouse and processed using ImageJ. **(A)** A projection of maximum intensity of each pixel over all video frames yielded faint outlines of active cells. **(B)** A time series of intensity, measured in 8-bit pixel values, for a region of interest (circled in green in A) thought to be a neuron upon visual inspection of the video. Blue arrow indicates likely spikes in activity of the neuron **(C)** A time series of intensity, measured in 8-bit pixel values, for region of interest not thought to contain a neuron upon visual inspection of the video (circled in red in A). All videos had a 30Hz frame rate.

CaImAn parameter optimization for GCaMP data

The calcium imaging analysis suite CaImAn (Pnevmatikakis and Paninski, 2013; Pnevmatikakis et al., 2016; Pnevmatikakis and Giovannucci, 2017) was used to process the calcium activity videos collected from the GCaMP-expressing wildtype mice. Since there were a few variables within the analysis suite that needed to be optimized, we first performed a parameter sweep with these variables (see Methods for more details). The analysis corrected for motion artifacts and yielded spatial footprints. These footprints were visually compared to determine which set of parameters created footprints the best. For example, changing the value of g_sig from 2 to 5 yielded spatial footprints that were too large and led to inaccurate spatial footprints (white arrows in figure 15). The set of parameters that yielded the best spatial footprints were used for the rest of the analysis. In the following results, all video analyses were performed with gsiz = 2, gsig = 5, neurons_per_patch = 200, nb_patch = 16 (see Methods for explanation of parameters).

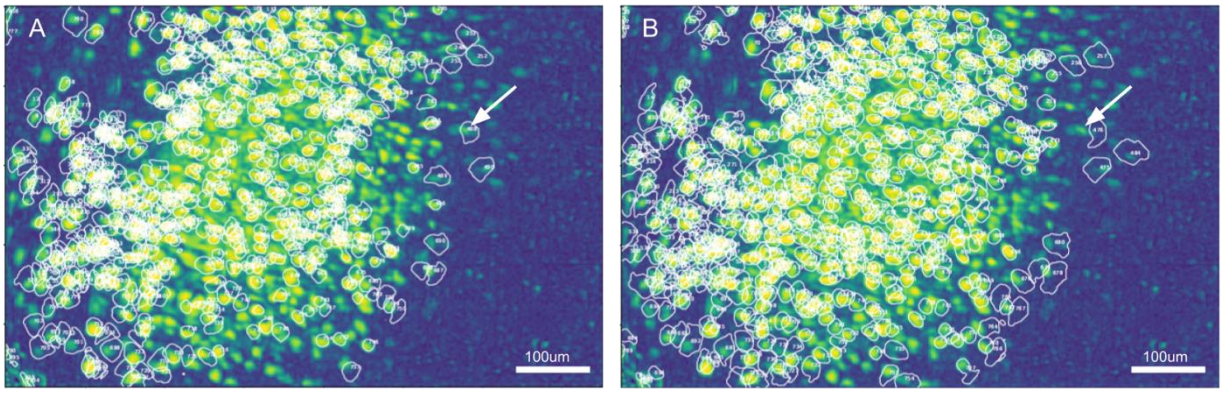

Figure 15. Comparison of spatial footprints generated from two sets of CaImAn parameters. 15 minutes of calcium activity from a GCaMP-expressing mouse was processed in CaImAn with the gsig variable set to either **(A)** 5 or **(B)** 8 while all other variables were held constant (see method for explanation of variables). The background image shows the spatiotemporal correlation of each pixel with its neighbors, with yellow indicating high correlation and blue indicating low correlation. Overlying white outlines are the spatial footprints generated by CaImAn. White arrows point to the same neuron in both (A) and (B). Scale bars indicate 100um. All videos had a 30Hz frame rate.

GCaMP CaImAn analysis

The behavioural videos were used to generate a histogram of occupancy within each maze (figure 16A-B). We also calculated the animal's speed from the video and categorized the animal's behaviour within the maze as "in-motion", when moving greater than 0.10m/frame, or "stationary". The in-motion occupancy of the animal (figure 16C) was used later in normalizing all neural activity, to account for the sampling bias created by the animal's uneven occupancy.

Using the results of the parameter sweep, the entire multi-day data set for one GCaMP-expressing mouse was processed to generate a set of spatial outlines of active neurons. The fluorescent activity contained within each spatial footprint was then analyzed and the neural activity was extracted for each cell (figure 17A). Following normalization by in-motion occupancy, each cell's activity was correlated with the location of the animal during the recording session to yield place fields (figure 17B-E).

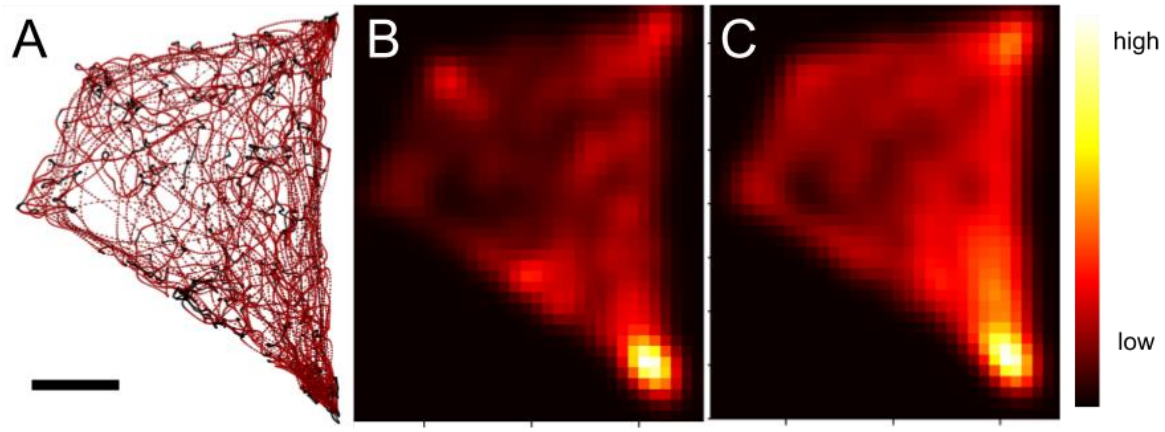

Figure 16. Tracking and occupancy data from behavioural videos. Behavioural videos recorded for each maze for one animal was analyzed to yield: **(A)** Red lines indicate animal trajectory, black indicates positions where animal was stationary during the entire behaviour recording. **(B)** Histogram of animal's occupancy within the maze. **(C)** Histogram of animal's occupancy within the maze only when moving. Scale bar indicates 20cm.

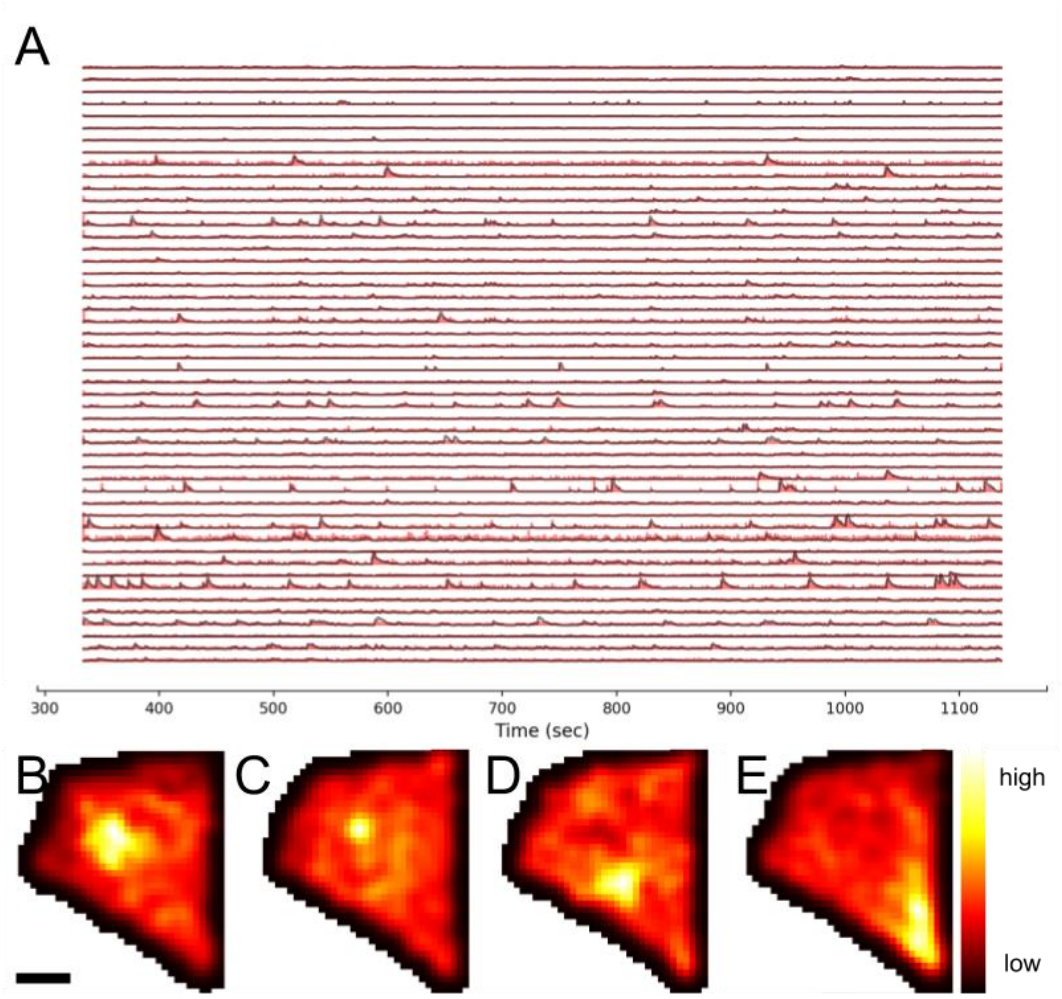

Figure 17. Inferred neural activity from CaImAn. Calcium activity recorded over a period of eleven days for one animal was processed by CaImAn **(A)** Sample of activity inferred from CaImAn. Each line represents one cell. Black lines are the denoised calcium concentration calculated from CaImAn, while red lines are the inferred spiking activity. **(B-E)** Four cells that showed spatially-tuned inferred spiking. The highest relative spiking rate for each cell is represented by bright yellow, while the lowest relative spiking rate is dark red. Each individual neuron's activity is normalized to the animal's in-motion occupancy within the maze. Maze shape is outlined in black. Scale bar indicates 20 cm.

Comparison with another method of analysis

We compared our CaImAn-generated place fields with place fields generated from a different analysis of calcium activity (Ziv et al., 2013). Data from the GCaMP-expressing animal during one session of one day was processed by both analyses (see Methods for details) and place fields were created from the spiking activity extracted (fig. 18). The analysis method by Ziv et al (2013) seems to have identified more instances of high activity, which can be seen in the multiple local clusters of yellow pixels in figure 18.

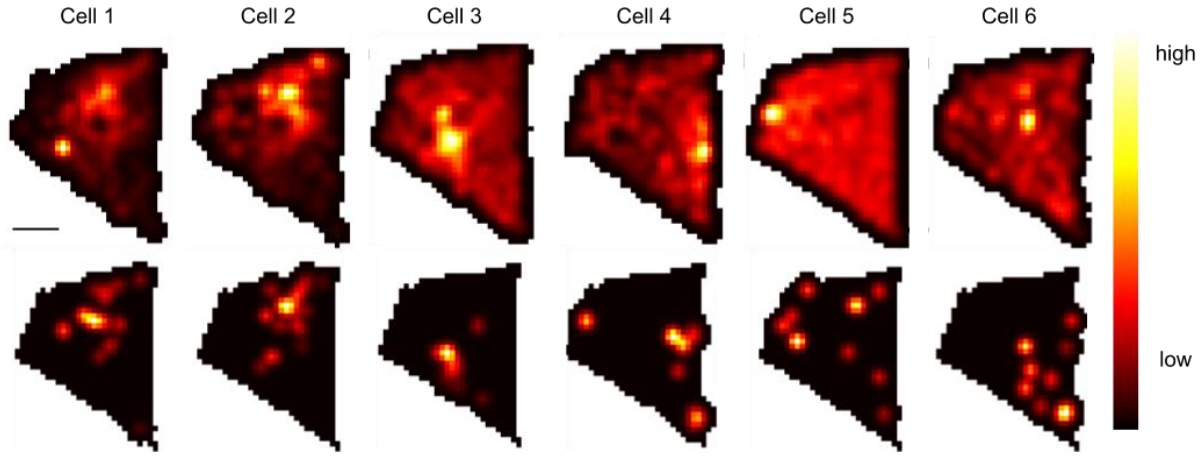

Figure 18. Comparison of place fields generated from two different analysis methods. The same day's data was processed using two different analyses (see methods for details). Top row is CaImAn. Bottom row is Ziv. Scale bar indicates 20cm.

Multi-day cell tracking

With the CaImAn-generated spatial footprints for each day's calcium videos, we used the CellReg analysis package (Sheintuch et al., 2017) to track cells within the video frame across days (see Methods for details). The place fields of the same cell between multiple days within the same environment were then compared to each other (figures 19).

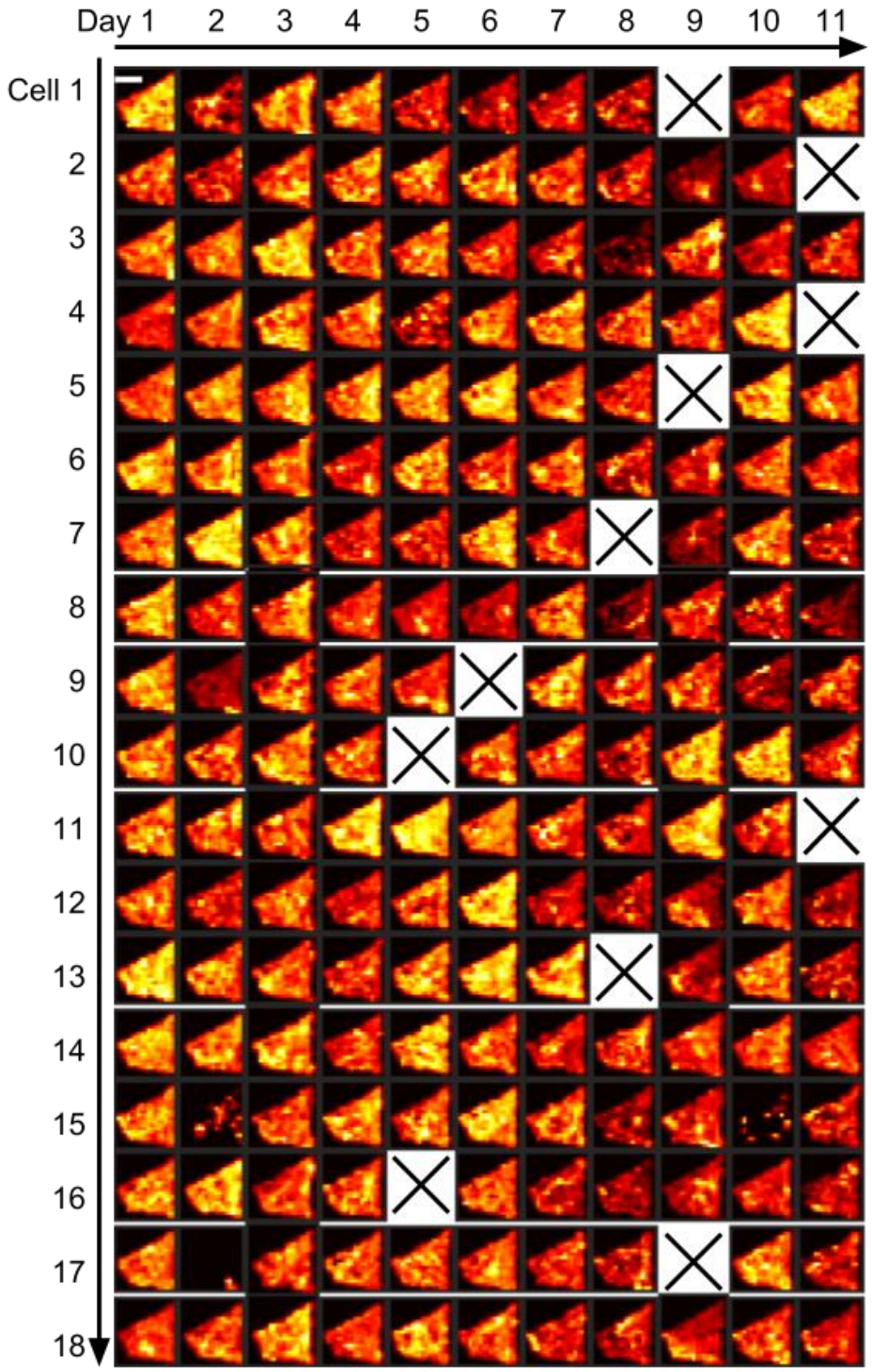

Figure 19. Place fields of cells that were detected in 10 or more days of recording. Calcium activity recorded over a period of eleven days for one animal was processed by CaImAn and CellReg was used to track cells across all days (see methods for details). The highest relative spiking rate for each cell is represented by bright yellow, while the lowest relative spiking rate is dark red. Each individual neuron's activity is normalized to the animal's in-motion occupancy within the maze. Scale bar at top left indicates 40cm.

Discussion

The goal of this project was to investigate how local inhibitory input to place cells might affect the stability of existing place fields. This would provide a mechanistic explanation for time course and conditions allowing the formation of place fields described in previous studies. Many previous studies have manipulated place cell activity directly (Lee et al., 2012). However, very few studies have looked into how interneurons, which provide all inhibitory input into place cells, can influence place field formation. One study that optogenetically inhibited interneuron firing in CA1 demonstrated that decreased inhibition is not sufficient to induce formation of new place fields and suggested that it is instead an increased inhibition of place cells that leads to place fields developing (Schoenenberger et al., 2016). To test this hypothesis, we used a combination of optogenetics and calcium imaging in a mouse model to simultaneously excite interneurons and record place cell activity.

Observations on implementing calcium imaging

The first aim of this project was to successfully implement calcium imaging with a green fluorescent calcium indicator (GCaMP6f) in an animal exploring an open field maze to verify our experimental technique. Calcium imaging enables long-term observation of the same cells and yields a larger cell population in comparison to electrophysiological recordings (Ghosh et al., 2011). Since calcium imaging had not been attempted in the Wilson lab prior to these experiments, we wanted to begin with a simplified experimental paradigm to have more confidence in troubleshooting our experimental technique. Although our formal experimental design used a red fluorescent calcium indicator (jRCaMP1b), we started with GCaMP6f because it has ~10x greater maximal fluorescence signal in comparison to jRCaMP6f and also a faster signal decay time (Chen et al., 2013; Dana et al., 2016). This meant that the fluorescent signals collected would be easier to see in real-time during experimentation and to extract neural spiking activity from using the

deconvolutional methods. Similar to previous studies monitoring neural activity through calcium imaging (Ghosh et al., 2011; Chen et al., 2013), the videos collected from the miniscope showed active GCaMP6f-expressing neurons whose fluorescent signal correlated with animal behavior (figure 12). Inspecting the changes in fluorescent intensity throughout the field of view revealed regions that had greater changes in intensity (figure 12), which we assumed to be active neurons.

A major weakness of using calcium indicators to measure neural activity is how slow the calcium and calcium indicator dynamics are in comparison to an action potential. Once an action potential reaches the axon terminal, voltage-gated calcium channels open and there is an influx of calcium ions that diffuses up to the soma. This influx takes around 10 milliseconds and levels within the cell drop back to baseline 60 milliseconds after the channels are opened (Lin and Schnitzer, 2016). In addition to the slow dynamics of somatic calcium concentration, dendritic fluorescence could overlap with fluorescing cells to introduce noise to the data and the fluorescent indicator itself is slow. When there is sufficient calcium within the cell, it takes less than a second for the calcium to bind to the calcium indicator to induce increased fluorescence (Lin and Schnitzer, 2016). In comparison, somatic action potentials are on the order of one millisecond long and place cells can fire action potentials at 10Hz or more (Lever et al., 2002). The slow dynamics of the calcium indicators therefore mask quick firing rates and make it essentially impossible to precisely measure the millisecond-to-millisecond changes in activity. The techniques we employed to extract approximate spiking activity from calcium indicators attempt to deconvolve the action potential rate from slow calcium dynamics (Pnevmatikakis and Paninski, 2013; Pnevmatikakis et al., 2016) using heuristic constraints on firing sparsity, signal noise, and calcium indicators dynamics. However, these algorithms are highly reliant on correct parameter choices (see methods for

details), and we did not have the resources to pursue a truly exhaustive and principled parameter sweep.

The slow fluorescence was partly why we chose not to continue with RCaMP analysis, but it also has implications for our GCaMP analysis. As place field detection relies heavily on aligning neural activity with animal position, there is a greater risk of a small offset in alignment resulting in incorrect place fields. Therefore, place fields generated from any type of calcium indicator activity will have a lower spatial resolution than ones generated from electrophysiological recordings and rely heavily on correct alignment of activity with location.

Optogenetics implementation needs to be confirmed with electrophysiology

Aside from the poor fluorescent signal of jRCaMP1b mentioned in the previous paragraph and in figure 12, another aspect of the RCaMP experimental technique should also be addressed. The transgenic mice expressing ChR2 in a subset of neurons were bred from well-established strains of mice from Jackson Laboratories (Vong et al., 2011; Madisen et al., 2012) and there was ChR2 expression within the expected brain regions (figure 13), but we were not able to confirm the functionality of the ChR2 being expressed. To verify ChR2 function, one can use electrophysiology to record cellular activity in the hippocampus and compare population activity levels when optogenetic stimulation is being delivered versus when it isn't. The challenge in performing electrophysiology and calcium imaging simultaneously in our model was that the design of the miniscope made it difficult to include an electrode interface. The miniscope was attached and detached from the baseplate daily, so as to reduce the burden on the animal, so any electrodes implanted would need to be wireless or have some auxiliary connector. Since a GRIN lens is placed directly above the tissue being stimulated, it would be hard to monitor population activity via surface electrodes or wireless electrode arrays, as other studies have done (Greenberg et al., 2008;

Bonfanti et al., 2012). Therefore, future studies looking to verify the ChR2 functionality could consider using electrodes implanted alongside the GRIN lens that have a sturdy connector which can be plugged in for each recording session.

Aberrant activity seen in GCaMP data

We also ran into a seemingly fundamental issue with endoscopic calcium imaging. Large, synchronized fluorescence were observed spreading like a spatial wave through the field of view sporadically through all recording sessions (Figure 20). These waves of fluorescence were most likely due to neural activity but were not consistent with previous reports of place cell activity. Bursts happened periodically throughout the entire behavioural session. Inspecting animal position

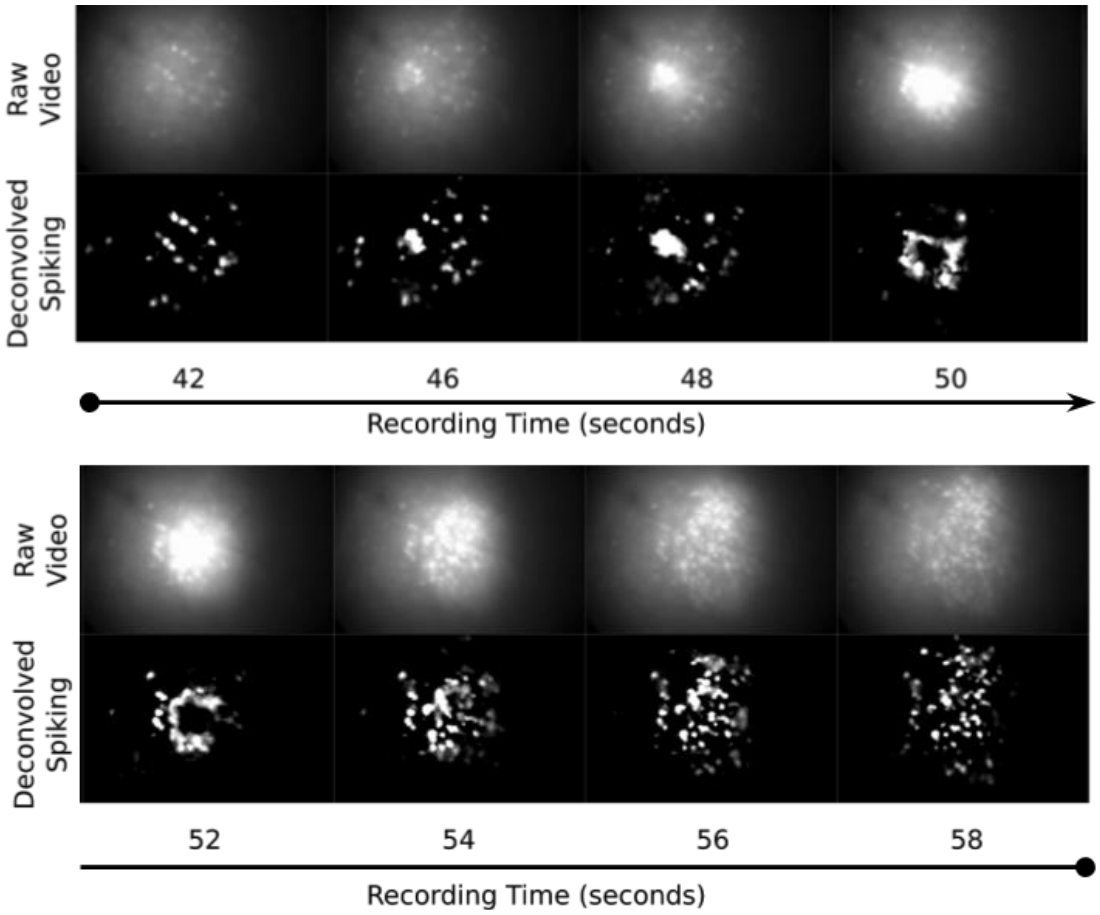

Figure 20. Progression of large, synchronized fluorescence through the imaging camera's field of view. Top of each vertical pair shows frames of raw video at 4 second intervals. Bottom each vertical pair shows the denoised video that was used to extract deconvolved spikes using CaImAn.

2 seconds before and after the onset of each burst did not reveal any position or activity-dependent correlates (figure 21). The frequency of bursting also varied between recording sessions (figure 22), with each burst lasting around 10 seconds.

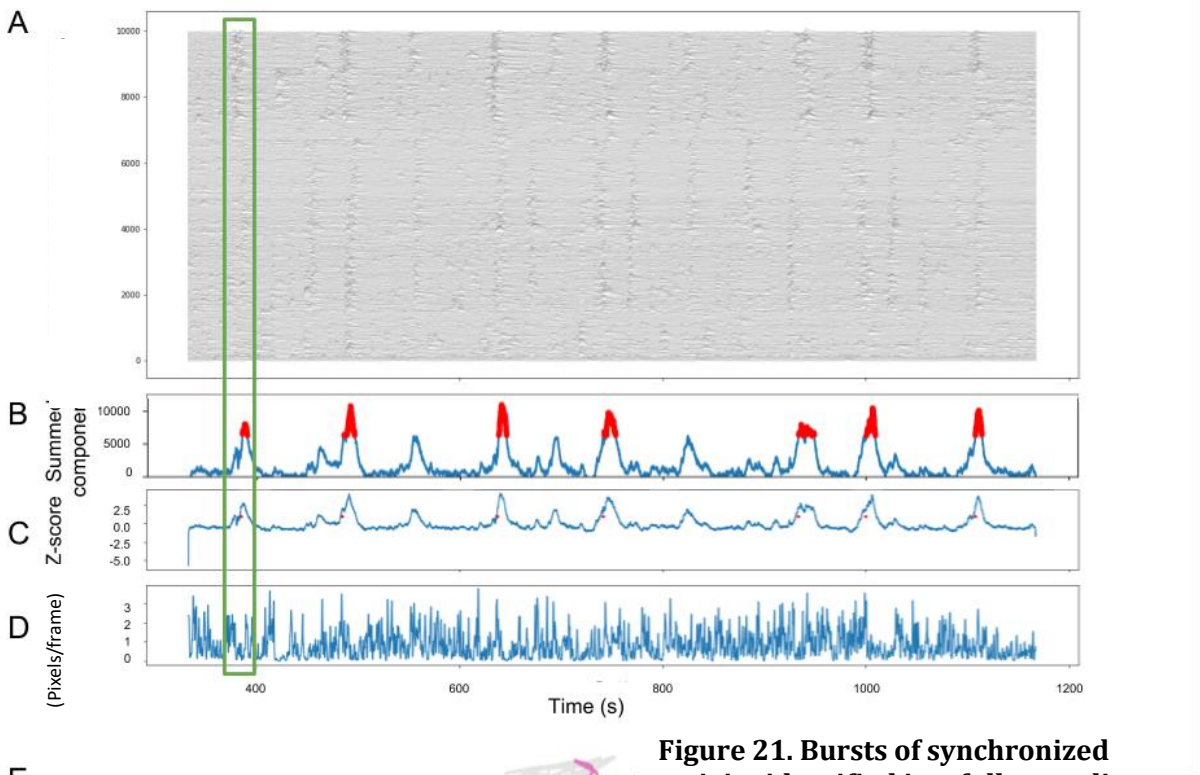

Figure 21. Bursts of synchronized activity identified in a full recording session. (A) Denoised calcium concentration, for the first 400 spatial components extracted from CaImAn **(B)** The sum of denoised calcium concentration of all spatial components extracted from CaImAn, measured in relative units, red points indicate where Z-score>2 **(C)** Z-score of the sum displayed in B, red points indicate the start of every burst period identified, set as whenever the Z-value became greater than 2 **(D)** Animal speed, smoothed over a Hann window 50 frames long, measured in pixels per frame **(E)** Animal position during the entire recording session (grey) and 2 seconds before and after the onset of each burst (coloured). Scale bar represents 20cm. Data shown is from the same recording session as figure 20. Burst displayed in figure 20 is outlined in panels A-D by a green box.

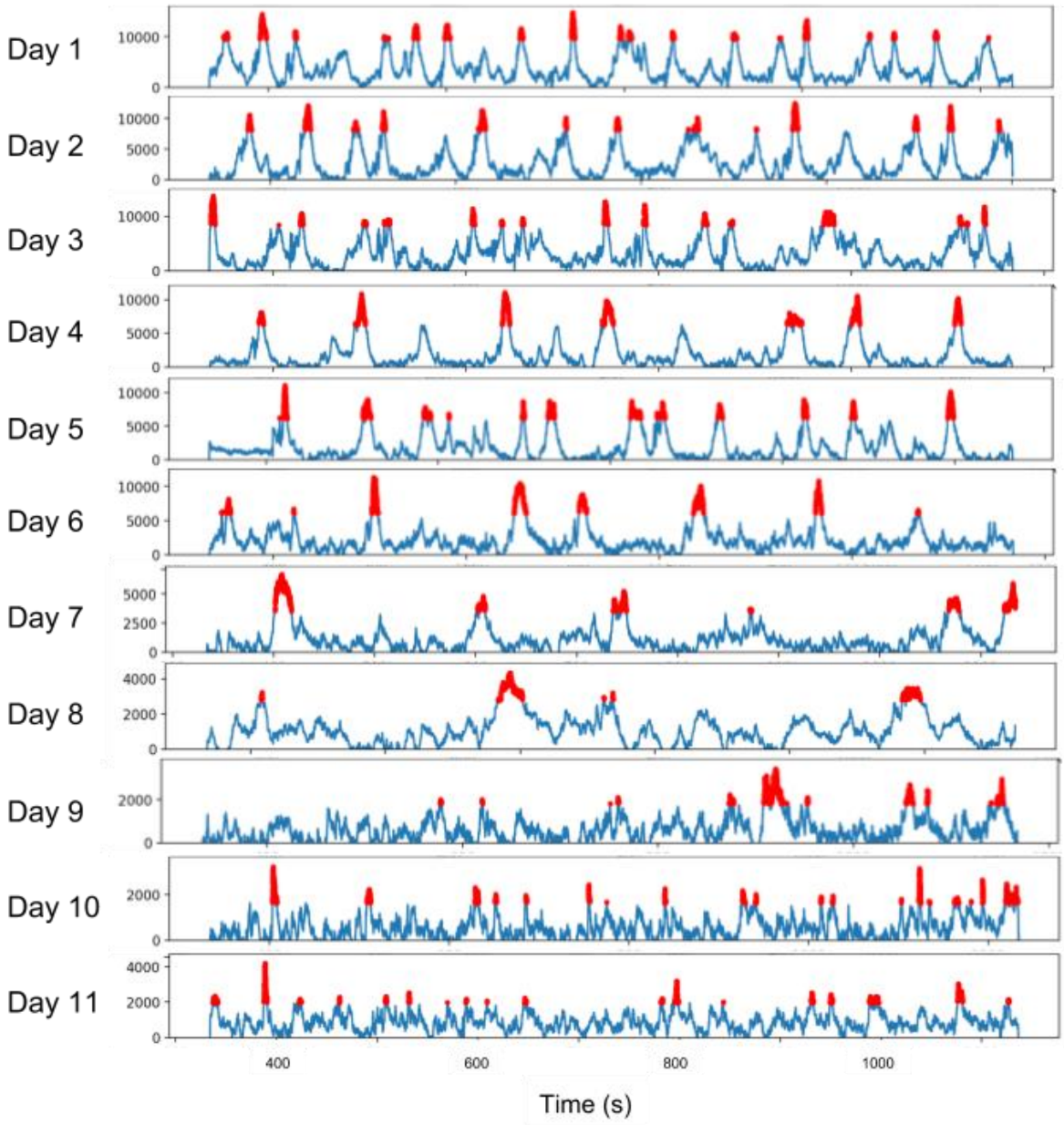

Figure 22. Bursts of synchronized activity identified in multiple recording sessions. The sum of the denoised calcium concentrations of all spatial components extracted from CaImAn for multiple days of recording in the same environment. Red points indicate where Z>2, in relative units.

These bursts may be due to aberrant large-scale synchronized activity. While there are not many reports of circuit instability due to the expression of GCaMP, a study looking into the long-term effects of transgenic expression of the family of GCaMP6 calcium indicators, which includes

GCaMP6f, also reported aberrant epileptic events confirmed via electrophysiology (figure 23, Steinmetz et al., 2017).

Various strains of transgenic mice were bred to express GCaMP in a subtype of cells. Researchers observed epileptic events in multiple brain regions of some animals and these events were also, in rare instances, correlated with behavioral tonic-clonic seizures in one transgenic mouse strain. Since the study used transgenic mice expressing GCaMP6, the researchers controlled for the effects of GCaMP expression during development in a subset of animals. These transgenic animals were given doxycycline to inhibit GCaMP expression until adulthood and did not exhibit seizure-like neural activity for 30 weeks following doxycycline removal. This contradicts our observations, as the lack of GCaMP expression during the mouse's adolescence did not prevent aberrant bursting activity. Additionally, the mouse we used was wildtype, so effects of other genetic manipulation are not relevant here.

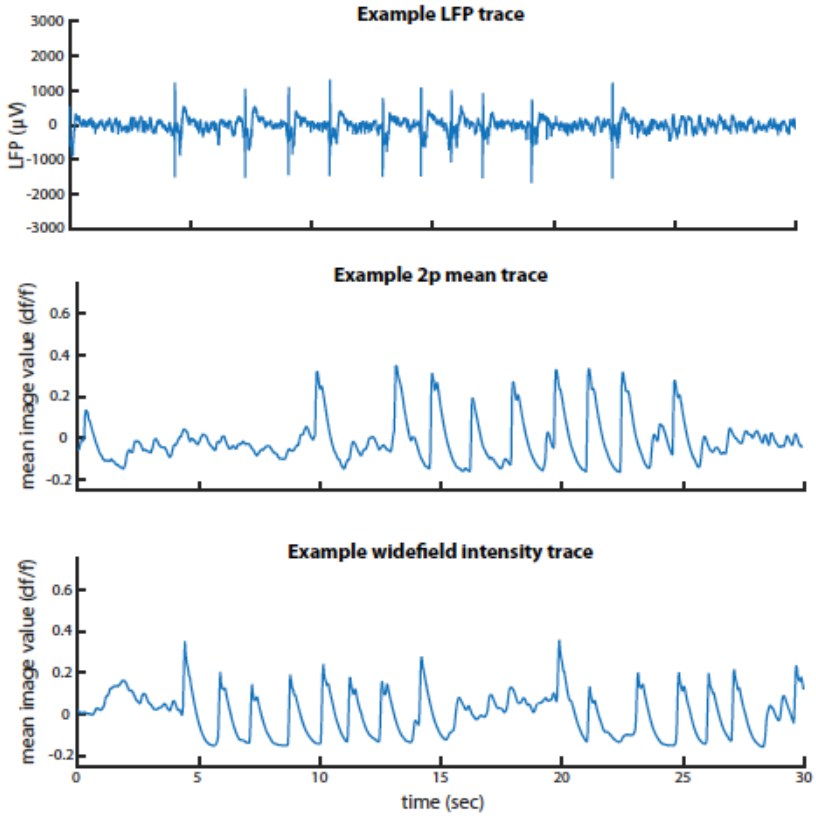

Figure 23. Traces of epileptiform activity from Steinmetz et al (2017). Epileptiform events observed in LFP, two photon calcium imaging, and widefield calcium imaging in one individual mouse, but not simultaneously. The genotype of the mouse was Emx1-Cre;Camk2a-tTA;Ai94 (expressing GCaMP6s). Two-photon trace was generated as the mean intensity of each frame across the entire field of view; widefield trace was generated as the mean within an ROI approximating the two-photon field of view. Each row contains an example trace from the same mouse. Figure and caption adapted from Steinmetz et al, 2017.

An important difference to note between our observed aberrant activity and the activity seen by Steinmetz and colleagues is that the time scale of our abnormal activity is much longer than that of Steinmetz et al (2017). While they observed 7 distinct peaks in activity within 10 seconds (figure 23), our abnormal activity occurred on the timescale of seconds rather than milliseconds (figure 21). Therefore, there needs to be further investigations into whether the abnormal activity seen in our data is the same activity reported by Steinmetz and colleagues.

This aberrant activity being seen in our GCaMP mouse could be explained by the effects of increased calcium levels within the cell, due to it binding to GCaMP. Calcium is an important secondary messenger within the cell and takes part in affecting gene expression for synaptic plasticity (West et al., 2001). Data from Steinmetz et al. (2017) support this theory, as greater and more diffuse expression of GCaMP was correlated with more aberrant activity.

The implications of aberrant activity on our collected is two-fold. First, these synchronized waves of activity were not excluded in our analysis and could have affected the place fields generated from the analysis. This could have influenced our interpretations of changes in place fields and resulted in false conclusions. Secondly, the aberrant activity could have had a behavioral effect on the mouse. While the mice in the Steinmetz study did not seem to have cognitive deficits related to the aberrant activity, they only studied activity on the surface of the brain. Our own observations of the mouse have yielded no signs of aberrant activity resulting in abnormal behaviour, but our observations are qualitative and may have a sampling bias. Therefore, follow-up projects could investigate how early these aberrant activities start, as our behavioral experiments started 2-3 months after GCaMP6f was injected, and whether there are behavioral or cognitive deficits related to these aberrant activities that could affect our study of spatial memory.

Comparing methods of extracting spiking activity

One last point of interest was revealed when comparing the CaImAn-generated place fields with place fields generated by the method by Ziv et al. (2013). Whereas CaImAn aimed to extract individual spikes from the calcium fluorescence recorded, Ziv et al (2013) worked with the assumption that place cells spike in bursts and therefore identifying these bursts of activity would be equivalent to finding the cell's periods of high activity. The CaImAn method detected a smoother gradient of activity from the raw data than the analysis by Ziv et al (2013), which made it both easier and harder to identify cells that had a place preference. While the colour contrast was decreased due to the smoother gradient of activity detected, the overall place preference of the cell is more apparent. When the same cells' activity was analyzed by the alternate method, activity was much sparser and therefore created more contrast within the heat map. Some cells retained their place preference, but other cells lost their place preference (Figure 18, cells 4-6). This sparser detection is likely because the alternate analysis did not infer spiking activity. Instead, action potentials were defined as instances where the fluorescence was two standard-deviations brighter than average. Although neither analysis can be deemed more "correct" than the other, it is important to acknowledge that the analyses used to analyze neural activity in calcium imaging could influence its interpretation.

Concluding remarks

This project successfully implemented calcium signaling in a mouse model using GCaMP6f. While the jRCaMP1b data was not processed due to timing constraints, continuations of this project should include performing a parameter sweep for RCaMP data, followed by analysis of multi-day neural activity, similar to what was outlined in this thesis. Other avenues of exploration include verifying the use of optogenetics in transgenic animals and investigating the aberrant activity seen in our GCaMP data.

References

Annese J, Schenker-Ahmed NM, Bartsch H, Maechler P, Sheh C, Thomas N, Kayano J, Ghatan A, Bresler N, Frosch MP, Klaming R, Corkin S (2014) Postmortem examination of patient H.M.'s brain based on histological sectioning and digital 3D reconstruction. Nat Commun 5.

Bannerman DM, Deacon RMJ, Offen S, Friswell J, Grubb M, Rawlins JNP (2002) Double dissociation of function within the hippocampus: Spatial memory and hyponeophagia. Behav Neurosci 116:884–901.

Bonfanti A, Ceravolo M, Zambra G, Gusmeroli R, Baranauskas G, Angotzi GN, Vato A, Maggiolini E, Semprini M, Spinelli AS, Lacaita AL (2012) A Multi-Channel Low-Power System-on-Chip for in Vivo Recording and Wireless Transmission of Neural Spikes. J Low Power Electron Appl 2:211–241 Available at: http://www.mdpi.com/2079-9268/2/4/211/.

Boyden ES, Zhang F, Bamberg E, Nagel G, Deisseroth K (2005) Millisecond-timescale, genetically targeted optical control of neural activity. Nat Neurosci 8:1263–1268.

Cai DJ et al. (2016) A shared neural ensemble links distinct contextual memories encoded close in time. Nature 534:115–118.

Chen T-W, Wardill TJ, Sun Y, Pulver SR, Renninger SL, Baohan A, Schreiter ER, Kerr RA, Orger MB, Jayaraman V, Looger LL, Svoboda K, Kim DS (2013) Ultrasensitive fluorescent proteins for imaging neuronal activity. Nature 499:295–300 Available at: http://www.nature.com/doifinder/10.1038/nature12354.

Cogan SF (2008) Neural Stimulation and Recording Electrodes. Annu Rev Biomed Eng 10:275–309 Available at: http://www.annualreviews.org/doi/10.1146/annurev.bioeng.10.061807.160518.

Corkin S (2002) What's new with the amnesic patient H.M.? Nat Rev Neurosci 3:153–160.

Dana H, Mohar B, Sun Y, Narayan S, Gordus A, Hasseman JP, Tsegaye G, Holt GT, Hu A, Walpita D, Patel R, Macklin JJ, Bargmann CI, Ahrens MB, Schreiter ER, Jayaraman V, Looger LL, Svoboda K, Kim DS (2016) Sensitive red protein calcium indicators for imaging neural activity. Elife 5.

Epsztein J, Brecht M, Lee AK (2011) Intracellular Determinants of Hippocampal CA1 Place and Silent Cell Activity in a Novel Environment. Neuron 70:109–120.

Ghosh KK, Burns LD, Cocker ED, Nimmerjahn A, Ziv Y, Gamal A El, Schnitzer MJ (2011) Miniaturized integration of a fluorescence microscope. Nat Methods 8:871–878.

Greenberg DS, Houweling AR, Kerr JND (2008) Population imaging of ongoing neuronal activity in the visual cortex of awake rats. Nat Neurosci 11:749–751 Available at: http://www.nature.com/doifinder/10.1038/nn.2140.

Hasselmo ME, Bodelón C, Wyble BP (2002) A Proposed Function for Hippocampal Theta Rhythm: Separate Phases of Encoding and Retrieval Enhance Reversal of Prior Learning. Neural Comput 14:793–817 Available at: http://www.mitpressjournals.org/doi/10.1162/089976602317318965.

Jeffery KJ, O'Keefe JM (1999) Learned interaction of visual and idiothetic cues in the control of place field orientation. Exp Brain Res 127:151–161.

Jezek K, Henriksen EJ, Treves A, Moser EI, Moser MB (2011) Theta-paced flickering between place-cell maps in the hippocampus. Nature 478:246–249.

Kim T Il et al. (2013) Injectable, cellular-scale optoelectronics with applications for wireless optogenetics. Science (80-) 340:211–216.

Lee D, Lin BJ, Lee AK (2012) Hippocampal place fields emerge upon single-cell manipulation of excitability during behavior. Science (80-) 337:849–853.

Lever C, Wills T, Cacucci F, Burgess N, O'Keefe J (2002) Long-term plasticity in hippocampal place-cell representation of environmental geometry. Nature 416:90–94.

Lin MZ, Schnitzer MJ (2016) Genetically encoded indicators of neuronal activity. Nat Neurosci 19:1142–1153.

Lopes G, Bonacchi N, FrazÃ£o J, Neto JP, Atallah B V., Soares S, Moreira L, Matias S, Itskov PM, Correia PA, Medina RE, Calcaterra L, Dreosti E, Paton JJ, Kampff AR (2015) Bonsai: an event-based framework for processing and controlling data streams. Front Neuroinform 9 Available at: http://journal.frontiersin.org/article/10.3389/fninf.2015.00007/abstract.
Maaswinkel H, Whishaw IQ (1999) Homing with locale, taxon, and dead reckoning strategies by foraging rats: Sensory hierarchy in spatial navigation. Behav Brain Res 99:143–152.
Madisen L et al. (2012) A toolbox of Cre-dependent optogenetic transgenic mice for light-induced activation and silencing. Nat Neurosci 15:793–802.
Morris RGM, Garrud P, Rawlins JNP, O'Keefe J (1982) Place navigation impaired in rats with hippocampal lesions. Nature 297:681–683.
Muller RU, Kubie JL (1987) The effects of changes in the environment on the spatial firing of hippocampal complex-spike cells. J Neurosci 7:1951–1968.
Nakai J, Ohkura M, Imoto K (2001) A high signal-to-noise ca2+ probe composed of a single green fluorescent protein. Nat Biotechnol 19:137–141.
Newman JP, Fong M, Millard DC, Whitmire CJ, Stanley GB, Potter SM (2015) Optogenetic feedback control of neural activity. Elife 4 Available at: http://elifesciences.org/lookup/doi/10.7554/eLife.07192.
O'Keefe J, Burgess N (1996) Geometric determinants of the place fields of hippocampal neurons. Nature 381:425–428.
O'Keefe J, Dostrovsky J (1971) The hippocampus as a spatial map. Preliminary evidence from unit activity in the freely-moving rat. Brain Res 34:171–175.
Pachitariu M, Steinmetz NA, Kadir SN, Carandini M, Harris KD (2016) Fast and accurate spike sorting of high-channel count probes with KiloSort. Adv Neural Inf Process Syst 29:4448–4456 Available at: https://papers.nips.cc/paper/6326-fast-and-accurate-spike-sorting-of-high-channel-count-probes-with-kilosort.pdf.
Patil AC, Thakor N V. (2016) Implantable neurotechnologies: a review of micro- and nanoelectrodes for neural recording. Med Biol Eng Comput 54:23–44.
Pnevmatikakis EA, Giovannucci A (2017) NoRMCorre: An online algorithm for piecewise rigid motion correction of calcium imaging data. J Neurosci Methods 291:83–94.
Pnevmatikakis EA, Soudry D, Gao Y, Machado TA, Merel J, Pfau D, Reardon T, Mu Y, Lacefield C, Yang W, Ahrens M, Bruno R, Jessell TM, Peterka DS, Yuste R, Paninski L (2016) Simultaneous Denoising, Deconvolution, and Demixing of Calcium Imaging Data. Neuron 89:299.
Pnevmatikakis E, Paninski L (2013) Sparse nonnegative deconvolution for compressive calcium imaging: algorithms and phase transitions. Adv Neural Inf …:1–9 Available at: http://papers.nips.cc/paper/4996-sparse-nonnegative-deconvolution-for-compressive-calcium-imaging-algorithms-and-phase-transitions.
Rich PD, Liaw HP, Lee AK (2014) Large environments reveal the statistical structure governing hippocampal representations. Science (80-) 345:814–817.
Rosenbaum RS, Priselac S, Köhler S, Black SE, Gao F, Nadel L, Moscovitch M (2000) Remote spatial memory in an amnesic person with extensive bilateral hippocampal lesions. Nat Neurosci 3:1044–1048.
Schindelin J, Arganda-Carreras I, Frise E, Kaynig V, Longair M, Pietzsch T, Preibisch S, Rueden C, Saalfeld S, Schmid B, Tinevez JY, White DJ, Hartenstein V, Eliceiri K, Tomancak P, Cardona A (2012) Fiji: An open-source platform for biological-image analysis. Nat Methods 9:676–682.
Schoenenberger P, O'Neill J, Csicsvari J (2016) Activity-dependent plasticity of hippocampal place maps. Nat Commun 7:11824 Available at: http://www.nature.com/doifinder/10.1038/ncomms11824.
Sheintuch L, Rubin A, Brande-Eilat N, Geva N, Sadeh N, Pinchasof O, Ziv Y (2017) Tracking the Same Neurons across Multiple Days in Ca2+ Imaging Data. Cell Rep 21:1102–1115.
Smith M Lou (1988) Recall of spatial location by the amnesic patient H.M. Brain Cogn 7:178–183.

Steinmetz NA et al. (2017) Aberrant Cortical Activity in Multiple GCaMP6-Expressing Transgenic Mouse Lines. eneuro 4:ENEURO.0207-17.2017 Available at: http://eneuro.sfn.org/lookup/doi/10.1523/ENEURO.0207-17.2017.

Teng E, Squire LR (1999) Memory for places learned long ago is intact after hippocampal damage. Nature 400:675–677.

Vong L, Ye C, Yang Z, Choi B, Chua S, Lowell BB (2011) Leptin Action on GABAergic Neurons Prevents Obesity and Reduces Inhibitory Tone to POMC Neurons. Neuron 71:142–154.

West AE, Chen WG, Dalva MB, Dolmetsch RE, Kornhauser JM, Shaywitz AJ, Takasu MA, Tao X, Greenberg ME (2001) Calcium regulation of neuronal gene expression. Proc Natl Acad Sci U S A 98:11024–11031 Available at: http://www.pubmedcentral.nih.gov/articlerender.fcgi?artid=58677&tool=pmcentrez&rendertype=abstract.

Wilson M, McNaughton B (1993) Dynamics of the hippocampal ensemble code for space. Science (80-) 261:1055–1058 Available at: http://www.sciencemag.org/cgi/doi/10.1126/science.8351520.

Wilson M, McNaughton B (1994) Reactivation of hippocampal ensemble memories during sleep. Science (80-) 265:676–679 Available at: http://www.sciencemag.org/cgi/doi/10.1126/science.8036517.

Zhang F, Wang LP, Boyden ES, Deisseroth K (2006) Channelrhodopsin-2 and optical control of excitable cells. Nat Methods 3:785–792.

Zhang S, Manahan-Vaughan D (2015) Spatial olfactory learning contributes to place field formation in the hippocampus. Cereb Cortex 25:423–432.

Ziv Y, Burns LD, Cocker ED, Hamel EO, Ghosh KK, Kitch LJ, El Gamal A, Schnitzer MJ (2013) Long-term dynamics of CA1 hippocampal place codes. Nat Neurosci 16:264–266 Available at: http://dx.doi.org/10.1038/nn.3329.